Biogeosciences Discuss., 7, 565–630, 2010
www.biogeosciences-discuss.net/7/565/2010/

Biogeosciences Discussions

This discussion paper is/has been under review for the journal Biogeosciences (BG).
Please refer to the corresponding final paper in BG if available.

Fire dynamics during the 20th century simulated by the Community Land Model

S. Kloster[1], N. M. Mahowald[1], J. T. Randerson[2], P. E. Thornton[3], F. M. Hoffman[3], S. Levis[4], P. J. Lawrence[4], J. J. Feddema[5], K. W. Oleson[4], and D. M. Lawrence[4]

[1]Earth and Atmospheric Sciences, Cornell University, Ithaca, NY, USA
[2]Department of Earth System Science, University of California, Irvine, CA, USA
[3]Climate and Ecosystem Processes, Environmental Science Division, Oak Ridge National Laboratory, Oak Ridge, TN, USA
[4]Climate and Global Dynamics Division, National Center for Atmospheric Research, Boulder, CO, USA
[5]Department of Geography, University of Kansas, Lawrence, KA, USA

Received: 16 November 2009 – Accepted: 7 January 2010 – Published: 26 January 2010

Correspondence to: S. Kloster (sk993@cornell.edu)

Published by Copernicus Publications on behalf of the European Geosciences Union.

Abstract

Fire is an integral Earth System process that interacts with climate in multiple ways. Here we assessed the parametrization of fires in the Community Land Model (CLM-CN) and improved the ability of the model to reproduce contemporary global patterns of burned areas and fire emissions. In addition to wildfires we extended CLM-CN to account for fires related to deforestation. We compared contemporary fire carbon emissions predicted by the model to satellite based estimates in terms of magnitude, spatial extent as well as interannual and seasonal variability. Longterm trends during the 20th century were compared with historical estimates. Overall we found the best agreement between simulation and observations for the fire parametrization based on the work by Arora and Boer (2005). We obtain substantial improvement when we explicitly considered human caused ignition and fire suppression as a function of population density. Simulated fire carbon emissions ranged between 2.0 and 2.4 Pg C/year for the period 1997–2004. Regionally the simulations had a low bias over Africa and a high bias over South America when compared to satellite based products. The net terrestrial carbon source due to land use change for the 1990s was 1.2 Pg C/year with 11% stemming from deforestation fires. During 2000–2004 this flux decreased to 0.85 Pg C/year with a similar relative contribution from deforestation fires. Between 1900 and 1960 we simulated a slight downward trend in global fire emissions, which is explained by reduced fuels as a consequence of wood harvesting and partly by increasing fire suppression. The model predicted an upward trend in the last three decades of the 20th century caused by climate variations and large burning events associated with ENSO induced drought conditions.

1 Introduction

Fires occur in all major biomes and influence climate in multiple ways. Fires lead to the emissions of trace gases and aerosols into the atmosphere impacting atmospheric chemistry (Crutzen et al., 1979), atmospheric radiative properties (Penner et al., 1992), and cloud formation (Feingold et al., 2001; Andreae et al., 2004). In addition, fires impact land surface energy fluxes (Liu and Randerson, 2008) and influence species composition, including the balance between forest, shrub, and grass plant functional types (Bond et al., 2004; Chambers et al., 2005). At the same time, fires are regulated by climate and impacted by human activity (Power et al., 2008). Therefore, fires are an integral Earth System process, that might exert nonlinear feedbacks, which are at present not well understood due to their complexity (Bowman et al., 2009).

Progress in understanding and monitoring fires has been made in recent years by the use of satellite observations to derive global burned area estimates (Tansey et al., 2008; Giglio et al., 2006). Although global fire emission estimates have improved significantly with the use of satellite based burned area products, the uncertainty remains high at the regional scale, because of incomplete information and parametrization of fuel loads, combustion completeness, and emission factors (Kasischke and Penner, 2004). However, satellite based fire products that cover a multi-year timespan are valuable tools for evaluating the capability of fire models to simulate fires globally in terms of the spatial distribution as well as seasonal and interannual variations.

A few models have been developed to prognostically simulate fire distributions in global vegetation models. Thonicke et al. (2001) relate area burned and fire season length by an empirically derived relationship. Arora and Boer (2005) introduce a process based approach by parameterizing the area burned as a function of fire spread rate. Pechony and Shindell (2009) developed a global-scale fire parametrization for fire favourable environmental conditions based on water vapor pressure deficits. Given the complexity of fires, these global-scale models are necessarily incomplete and more data will be needed in the future to constrain better global general parametrizations of

BGD
7, 565–630, 2010

fire processes.

In this study we modified the global representation of fires in the biogeochemical model CLM-CN (Thornton et al., 2009) based on the work by Thonicke et al. (2001) and Arora and Boer (2005). Our goal in this study was to best match the observed spatial and temporal variability of fires for the contemporary time period, and predict how fires have changed over the historical record. In the deforestation process fire is often used as a tool for land clearing to facilitate agricultural usage (van der Werf et al., 2009). Deforestation fires contribute to contemporary fire emissions mainly in tropical regions (van der Werf et al., 2006; Page et al., 2002), but are a highly spatially variable source over the last century related to land use changes. In this study, we use the ability of CLM-CN to apply prescribed dynamic land use datasets to explicitly account for the fraction of deforestation which occurs through burning. This allows us to compare simulated contemporary fire carbon emissions to satellite based estimates, which monitor the combination of wildfires and deforestation fires. In addition, we estimate the change in total fires introduced by the variable deforestation rate over the last century by making use of land use transition scenarios (Hurtt et al., 2006). We also add the active role humans have in modulating wildfires either by adding an ignition source or by suppressing fires (Robin et al., 2006; Stocks et al., 2003) assuming that the parameters can be parametrized as a function of population density.

For this study we performed offline CLM-CN simulations for 1798 to 2004 and compared simulated contemporary area burned and fire carbon emissions to satellite based global fire products (van der Werf et al., 2006; Schultz et al., 2008; Tansey et al., 2008; Mieville et al., 2010) and analysed the trend in fire carbon emissions simulated over the last century. In addition, we performed several sensitivity studies to disentangle the impact of climate change, change in population density and land use change and wood harvest on the simulated fire carbon emissions to explain the simulated trend over the last century. Due to the limited time coverage of the re-analysis data used in this study to force CLM-CN (Qian et al., 2006) we only take into account varying climate between 1948 and 2004, which, however, includes most of the anthropogeni-

cally derived climate change. The results presented here are the first fully consistent modeling attempt to globally estimate changes in fires driven by changes in population density, land use and climate over such a long time period.

The paper is structured as follows: Sect. 2 briefly describes the model used in this study. A more detailed description of the different fire algorithms used and the treatment of deforestation fires can be found in the Appendix A; Sect. 3 summarizes the simulations performed in this study and the observations used for an evaluation of the results. Results for contemporary time periods are discussed and compared to observations in Sect. 4: Sect. 4.1 compares the simulated annual burned area and fire carbon emissions to recently developed satellite based fire products; Sect. 4.2 compares the simulated seasonal and interannual variability for fire carbon emissions to observed ones; Sect. 5 evaluates the trend in fire carbon emissions as simulated for the 20th century together with a sensitivity analysis of simulated fire carbon loss to climate, population density, and land use conversion (Sect. 5.1); Sect. 6 gives a summary of the results together with concluding remarks.

2 Model description

All simulations in this study were performed with a modified version of the Community Land Model version 3.5 (CLM3.5; Oleson et al., 2008b; Stoeckli et al., 2008). The modifications of the model physics beyond CLM3.5 incorporate most of the updates of the model that will make up CLM version 4 and include revisions to the hydrology scheme (Decker and Zeng, 2009; Sakaguchi and Zeng, 2009), a modified snow model including aerosol deposition, vertically resolved snow pack heating, a density-dependent snow cover fraction parametrization, and a revised snow burial fraction over short vegetation (Niu and Yang, 2007; Flanner and Zender, 2005, 2006; Flanner et al., 2007; Wang and Zeng, 2009; Lawrence and Slater, 2009), a representation of the thermal and hydraulic properties of organic soil (Lawrence and Slater, 2008a), a 20-m deep ground column (Lawrence et al., 2008b), and an urban model (Oleson et al., 2008a). The PFT dis-

tribution is as in Lawrence and Chase (2007) except that a new cropping dataset is used (Ramankutty et al., 2008) and a grass PFT restriction has been put in place to reduce a high grass PFT bias in forested regions by replacing the herbaceous fraction with low tress rather than grass. Taken together, the augmentations to CLM3.5 result in improved soil moisture dynamics that lead to higher soil moisture variability and drier soils. Excessively wet and unvarying soil moisture was recognized as a deficiency in CLM3.5 (Oleson et al., 2008b; Decker and Zeng, 2009). The revised model also simulates, on average, higher snow cover, cooler soil temperatures in organic-rich soils, higher global river discharge, lower albedos over forests and grasslands, and higher transition-season albedos in snow covered regions, all of which are improvements compared to CLM3.5.

Additionally, the model is extended with a carbon-nitrogen biogeochemical model (Thornton et al., 2007, 2009; Randerson et al., 2009) hereafter referred to as CLM-CN. CN is based on the terrestrial biogeochemistry Biome-BGC model with prognostic carbon and nitrogen cycle (Thornton et al., 2002; Thornton and Rosenbloom, 2005). CLM-CN dynamically accounts for carbon and nitrogen state variables and fluxes in vegetation, litter, and soil organic matter. It retains the prognostic estimation of water and energy in the vegetation-snow-soil column from CLM. Detailed description of the biogeochemical component of CLM-CN can be found in Thornton et al. (2007).

The original version of CLM-CN includes a prognostic treatment of fires based on the fire algorithm by Thonicke et al. (2001) (CLM-CN-T), which was originally developed for the LPJ (Lund-Potsdam-Jena) model (Sitch et al., 2003). In this study we modified the representation of wildland fires in CLM-CN by a fire algorithm based on the work by Arora and Boer (2005) (CLM-CN-AB), which was developed within the CTEM (Canadian Terrestrial Ecosystem Model) framework (Verseghy et al., 1993).

In both the Thonicke et al. (2001) and Arora and Boer (2005) algorithms, the first step is to estimate burned area using information about climate and fuel loads. Then fire carbon fluxes to the atmosphere (E) are related to combustion and mortality following:

$$E = A \cdot C \cdot \mathrm{cc} \cdot \mathrm{mort} \quad (1)$$

with A representing the area burned, C the carbon concentrations for the different fuel types considered in CLM-CN and cc and mort the combustion completeness and mortality factors that differ between different plant functional types considered in CLM-CN. While Thonicke et al. (2001) uses an empirical relationship relating fire season length and burned area, Arora and Boer (2005) introduces a process based fire parametrization simulating area burned as a function of fire spread rate. Both algorithms differ in their assumptions made for combustion completeness and mortality factors. The implementation of the two fire algorithms into CLM-CN are described in detail in the Appendix A.

We modified the dynamic land cover treatment in CLM-CN to account for deforestation fires in relation to fire probabilities simulated in the individual fire algorithms (details can be found in the Appendix A5). We further extended the CLM-CN-AB version by an explicit treatment of human ignition following Venesky et al. (2002), for which human ignition probability increases with population density. For fire suppression we also assume a population density dependency, with the highest fire suppression rate (90%) in densely populated areas. Details can be found in the Appendix A4.

3 Simulations and observations

We performed a series of simulations to test the performance of the two fire algorithms (Thonicke et al., 2001; Arora and Boer, 2005) implemented in CLM-CN in combination with several sensitivity simulations to disentangle the importance of the individual forcing factors (climate, population density, land use change and wood harvest) for the simulated burned area and fire carbon emissions. All simulations are offline simulations in which CLM-CN is forced by a prescribed data set of atmospheric fluxes and states. Table 1 summarizes the simulations performed for this study.

All simulations were branched from control simulations (205 years) using CLM-CN with the Thonicke et al. (2001) fire algorithm (C-T) or with the Arora and Boer (2005) fire algorithm (C-AB, C-AB-HI, C-AB-HI-FS) in which the model is in steady state with

respect to the prescribed forcing data. For our implementation of the Arora and Boer (2005) algorithm we assumed a constant human ignition probability as done in the original Arora and Boer (2005) publication (C-AB). Alternatively we introduced a human ignition probability as function of population density (C-AB-HI), and a human ignition probability in combination with human initiated fire suppression (C-AB-HI-FS). Appendix A4 in the appendix describes in detail how we parametrized human ignition and fire suppression as a function of population density. In all control simulations atmospheric CO_2 concentration, nitrogen deposition and land cover (Hurtt et al., 2006) are set to pre-industrial values. As climate forcing a repeating cycle of the first 25 years (1948–1972) of National Centers for Environmental Prediction/National Center for Atmospheric Research (NCEP/NCAR) reanalysis data (Qian et al., 2006) is used. The simulations that take into account human ignition and fire suppression as a function of population density (C-AB-HI and C-AB-HI-FS) used population density data representative for the year 1850 throughout the simulation period (Klein Goldewijk, 2001). We realized that the nitrogen deposition used in these simulations have a high global total (25%) compared to previous studies (Lamarque et al., 2005). Sensitivity studies with nitrogen depositions following Lamarque et al. (2005), that will be the standard field used in future CLM-CN simulations, showed changes in fire carbon emissions by less than 2% for the global total and only a few regions show higher deviations with a maximum not exceeding 10%.

Starting from the control simulations we conducted correspondent transient simulations (T-FULL, AB-FULL, AB-HI, AB-HI-FS) from 1798 to 2004 with transient time-varying atmospheric CO_2 concentrations, population density, nitrogen deposition, land use change and wood harvest and cyclic 1948–1972 NCEP/NCAR forcing until 1972. From 1973 onwards NCEP/NCAR forcing is used corresponding to the model simulation year as done in Randerson et al. (2009).

In addition to the transient simulations that were driven with the full set of transient forcings we performed a series of sensitivity simulations in which individual forcing factors are kept constant at their pre-industrial values. These include the simulation

AB-LUC in which land use change and wood harvest is kept constant at the 1850 value and AB-CLIM in which the NCEP/NCAR forcing uses the 25 year repeat cycle (1948–1972) throughout the simulation period. Two more sensitivity simulations were conducted for the case in which human ignition (AB-HI-PI) and human ignition and fire suppression (AB-HI-FS-PI) is taken into account as a function of population density using constant population density data representative for the year 1850.

To evaluate the simulated burned area and fire carbon emissions we used satellite based fire products for the contemporary period. The simulated trend over the 20th century is compared with estimates based on long-term historical observational records.

In recent years a number of global satellite derived burned area products have been developed, including GLOBSCAR (Simon et al., 2004), GBA2000 (Gregoire et al., 2002), GlobCarbon (Plummer et al., 2006), MODIS Collection 5 (Roy et al., 2008), L3JRC (Tansey et al., 2008), and GFEDv2 (Giglio et al., 2006). In this study we compare our results to the publicly available satellite based estimates reported in the Global Fire Emission Database (GFEDv2, van der Werf et al., 2006), the recently published L3JRC product (Tansey et al., 2008), and GICC estimates (Mieville et al., 2010) spanning multi-year time periods.

GFEDv2 reports area burned along with fire carbon emissions on a monthly basis with 1° by 1° resolution for the time period 1997–2004. Area burned estimates are derived for 2001 to 2004 from MODIS active fire observations and were extended back through 1997 using ATSR and VIRS satellite data (Giglio et al., 2006). The area burned estimates are embedded into a global biogeochemical model (CASA, Carnegie-Ames-Stanford Approach). Direct fire carbon emissions are calculated similar to the fire algorithms used in this study as product of area burned, available biomass, fire induced mortality, and a combustion completeness factor. L3JRC reports area burned with a resolution of 1 km for April 2000 to April 2007 on a daily basis using SPOT VEGETATION reflectance data in combination with a modified version of the Global Burnt Area 2000 (GBA2000) algorithm. Burned areas were evaluated for selected regions

with Landsat TM scenes revealing a significant underestimation of burned area in regions with low vegetation cover. GICC reports fire emissions on an annual basis for the period 1997–2005 based on satellite products (GBA2000 burned areas, ATSR fire counts), and on the Global Land Cover (GLC) 2000 vegetation map. Emissions are first estimated for year 2000 from GBA2000 burned areas as product of burned areas, biomass densities, burning efficiencies, and emission factors. ATSR fire counts are then used to derive temporal and spatial distribution of fire emissions from the GBA 2000 emissions for the period 1997–2004.

Notice that large discrepancies remain between the satellite based products (Boschetti et al., 2004; Roy and Boschetti, 2009; Chang and Song, 2009). Thus, while we compare our results to the best available observations, there remains a large uncertainty in any fire model evaluation, because of the large uncertainty in observations.

Long-term observations on fire activity are very sparse and related to high uncertainties especially at broad spatial scales (Marlon et al., 2008). Schultz et al. (2008) developed for the RETRO project a fire emission inventory for the period 1960 to 2000 based on different satellite products, a semi-physical fire model and an extensive literature review. We use this product for an evaluation of the mean state, the interannual variability, and the trend between 1960 and 2000. Mouillot et al. (2006) constructed a yearly global burned area product for the 20th century based on published data, land use practices, qualitative reports and local studies, such as tree ring analysis. Mieville et al. (2010) used these trends to derive decadal mean fire emissions by calculating the product of burned areas, biomass densities, burning efficiencies, and emission factors scaled to the contemporary GICC estimates. In the following we will refer to this product as GICChist.

4 Fires in the contemporary period

4.1 Annual area burned and carbon emissions

The global distribution of simulated annual area burned is compared for the simulations T-FULL and AB-HI-FS to estimates given in the L3JRC (Tansey et al., 2008) and GFEDv2 (van der Werf et al., 2006) fire products (Fig. 1). In general the model simulations are able to capture broad spatial patterns across continents. Annual burned areas during 1997–2004 range between 176 and 330 Mha in the model simulations, while GFEDv2 reports 329 Mha. For the period 2001–2004 the simulations vary between 175 and 321 Mha, while the L3JRC product estimates 401 Mha. Thus, the global annual model estimates are on the low side of observational estimates.

Regional averages suggest a large sensitivity of the modeled results to the fire formulations used (Fig. 2). Because of the large interannual variability in regional area burned, we show regional averages for the appropriate time periods for each of the satellite derived products. Figure A3 defines the regions used for this analysis.

Highest annual area burned is simulated over the African continent, which contributes between 33 and 40% to the global total, followed by South America (16 to 27% of the global total). L3JRC and GFEDv2 estimates vary considerably within these regions.

For Africa Table 2 compares annual area burned estimates and carbon emission from Northern and Southern Hemisphere Africa as reported in GFEDv2 and L3JRC averaged over the time period 2001–2004. While L3JRC reports the largest annual area burned in Southern Hemisphere Africa, GFEDv2 shows highest values for Northern Hemisphere Africa. A validation of MODIS, L3JRC and GlobCarbon burned-area products for Southern Hemisphere Africa using independent LANDSAT data revealed a particularly strong underestimation in area burned for the L3JRC product (Roy and Boschetti, 2009) as already noted by Tansey et al. (2008). Lehsten et al. (2009) corrected for this underestimation in the L3JRC product for Africa assuming that the tree and shrub cover classes are underestimated by 48 and 25%, respectively, resulting

BGD
7, 565–630, 2010

in a burned area that is approximately 25% higher than reported in L3JRC. A study from Ito et al. (2007) based on MODIS burned area reports an annual area burned of 200 Mha for Southern Hemisphere Africa for the same time period. Other estimates range between 58 and 226 Mha for Southern Hemisphere Africa (Ito et al., 2007, and references therein) and 136 and 362 Mha for Northern Hemisphere Africa (Schultz et al., 2008, and references therein). All CLM-CN simulations lead to a considerably lower annual burned area over the African continent (Northern Hemisphere: 19.5–44.5 Mha; Southern Hemisphere: 39.0–74.1 Mha).

For South America CLM-CN simulations lead to higher total annual area burned (31–82 Mha) compared to GFEDv2 (16.3 Mha) for the time period 1997–2004. L3JRC reports an annual area burned over South America (36.8 Mha) for the time period 2001–2004, which falls within the lower range of the simulations (28–80 Mha). Ito and Penner (2004) report for South and Central America for the year 2000 a burned area of 12.3 Mha based on GBA2000 and ATSR fire count data. GLOBSCAR and GBA2000 estimates are 13.8 and 11.9 Mha for South America (Kasischke and Penner, 2004).

There are discrepancies between the model and satellite observations in other regions, but the large difference between the satellite based estimates precludes an effective model evaluation in these regions. For example the model estimates for temperate North America range between 15 and 21 Mha area burned, compared with GFEDv2 estimates of 20 Mha and L3JRC estimates of 2.5 Mha. The model estimates burned area in boreal Asia between 1.5 and 6.6 Mha, while the observations are higher but with a large uncertainty (GFEDv2: 9.0 Mha, L3JRC: 42.1 Mha). Estimates reported in the literature for Russia, in which about two thirds of the world's boreal forests lie, range between 5.3 and 13.1 Mha (Soja et al., 2004, and references therein). Chang and Song (2009) found that the L3JRC product significantly overestimates the burned area in the northern high latitudes when compared with ground-based measurements and other satellite data. They related this overestimation to excessive detection of burned area during the period outside the fire season. Thus, it appears that the models underestimate boreal forest area burned extent, but the factor by which it underestimates area

burned is not clear.

Of all the simulations, T-FULL produces the smallest annual area burned globally. A higher annual area burned is simulated in the AB-FULL simulation. The best spatial correlation between simulation and GFEDv2 as well as L3JRC is found for the AB-HI-FS simulation (0.52 and 0.53, respectively). Taking into account human ignition and fire suppression explicitly as a function of population density (AB-HI-FS), improves the simulated annual area burned over densely populated regions such as India, Europe and the East coast of the USA in comparison to GFEDv2 and L3JRC. The impact of fire suppression and human ignition on the simulated burned area will be further discussed in Sect. 5.1.2.

Next we assess the modeled carbon losses due to fire against available observations. The global distribution of simulated annual fire carbon losses show a similar spatial pattern to estimates from GFEDv2 (van der Werf et al., 2006), GICC (Mieville et al., 2010) and RETRO (Schultz et al., 2008) (Fig. 3), although there are discrepancies. Regional averages, similar to those for burned area, show larger differences (Fig. 4).

The simulated total (wildfire and deforestation) fire carbon emissions range between 2.0 and 2.4 Pg C/year for the period 1997–2004. For the same period GFEDv2 and GICC report 2.3 and 2.7 Pg C/year, respectively. For the period 1960 to 2000 RETRO estimates fire carbon emissions to be 2.0 Pg C/year for which the simulations yield 1.7–2.2 Pg C/year. This suggests that the models yield reasonable estimates of global carbon loss over this time period. Similar to the area burned, the best spatial correlation between simulated fire carbon emissions and fire products is found in the AB-HI-FS simulation (Fig. 4).

While we find a large range of annual burned area in our different simulations, the total global carbon emissions are relatively similar. This non-linear relationship between burned area and fire carbon emissions is partly explained by different aboveground vegetation pools in steady state for the different simulations (Table 3). The different annual burned area simulated with the various model configurations has a large effect on

the modeled carbon stock in steady state. A high annual area burned (e.g. AB-FULL simulation) leads to a relatively low aboveground biomass carbon pool in steady state and thus lower fuels loads and carbon emissions per unit area burned. In contrast, a low annual area burned (e.g. T-FULL simulation) leads to a relatively high aboveground biomass carbon pool in steady state and thus to high rates of fire emissions. In addition, different assumptions about fire induced mortality and combustion completeness factors in the two different fire algorithms applied here (see Appendix A3) lead to different levels of fuel consumption. Also, different distributions of fires globally contribute to different global burned area to fire carbon emissions ratios, as area burned and carbon emissions are largely decoupled on a global scale (van der Werf et al., 2006).

Similar to the simulated area burned, modeled fire carbon emissions are too low over the African continent (738 to 1099 Tg C/year; GFED: 1190 Tg C/year, GICC: 1256 Tg C/year) and too high over South America (711 to 908 Tg C/year, GFED: 326 Tg C/year, GICC: 502 Tg C/year). For Africa Table 2 compares the simulated values for the period 2001 to 2004 with GFEDv2 and values given in Lehsten et al. (2009). Lehsten et al. (2009) utilized a bias corrected L3JRC area burned product for Africa to simulate fire carbon emissions within the LPJ-GUESS model (Smith et al., 2001) in a similar approach as described by van der Werf et al. (2006). Both, area burned and fire carbon emissions, are higher in Northern Hemisphere Africa compared to Southern Hemisphere Africa in GFEDv2, whereas Lehsten et al. (2009) find higher values in Southern Hemisphere Africa. The ratio between annual fire carbon emissions and area burned is 7.2 Tg C/Mha (NHAF) and 4.5 Tg C/Mha (SHAF) for GFEDv2, which is higher than in Lehsten et al. (2009) (4.1 and 3.2 Tg C/Mha, respectively). All CLM-CN simulations lead to significantly higher ratios. As a result the simulated fire carbon emissions become comparable or even exceed the Lehsten et al. (2009) values, although the annual area burned is simulated significantly lower.

Deforestation fires contribute between 141 (AB-FULL) and 204 (T-FULL) Tg C/year to the total carbon emissions (~6–9%) globally in the 1990s. This is about 34–42% of

the total conversion flux related to land use change. In our model, the fraction of the conversion of land that occurs by burning depends on fire probabilities as simulated in the fire algorithms (see Appendix A5). As a consequence, larger contributions are simulated in regions with relatively high fire probabilities such as Northern Hemisphere Africa (~70%) and lower contributions in regions with relatively low fire probabilities such as Europe (~30%).

4.2 Interannual and seasonal variability

Figure 5 shows the interannual variability in total (wildfire and deforestation) fire carbon emissions as simulated between 1997 and 2004 compared to estimates reported by GFEDv2 (van der Werf et al., 2006) and GICC (Mieville et al., 2010) for selected world regions, which are characterized by a high interannual variability (Table 4). Correlations between simulations and GFEDv2 and GICC for all world regions are listed in Table 4.

Considerable interannual variation is evident in regions, which are influenced for example by ENSO, for which the event of 1997/1998 was the most extreme during the last century (Glantz, 2001). Here the simulations capture the enhanced burned area and fire carbon emissions associated with El Niño induced drought conditions. For example for equatorial Asia enhanced fire carbon emissions are simulated in 1997 and to a lesser extent in 2002 in accordance with GFEDv2 and GICC estimates (correlation 0.95–1.00). Another peak is simulated in 1982/1983 which is consistent with observations (Schultz et al., 2008, not shown). In Central America fire carbon emissions peak in 1998 due to ENSO induced drought that resulted in catastrophic burning events in the tropical forest of Southern Mexico and Central America from April to June 1998 (Kreidenweis et al., 2001). Other large biomass burning events observed in boreal forests in summer 1998 (Kasischke and Bruhwiler, 2003) are reproduced by the simulations for boreal North America but are not captured for boreal Asia.

The simulation T-FULL underestimates interannual variability and has a lower correlation with GFEDv2 as well as GICC in many regions, including boreal North America, boreal Asia and Europe. Better results are obtained when the Arora and Boer (2005)

based algorithm is used in CLM-CN (simulations AB-FULL, AB-HI, AB-HI-FS). The explicit treatment of human ignition and fire suppression have only a small impact on the interannual variability between 1997 and 2004. Regions having poor correlation between simulations and GFEDv2 and GICC such as central Asia, Northern Hemisphere Africa and Southern Hemisphere Africa are characterized by a small interannual variability reported in GFEDv2 and GICC and are therefore hard to capture with our model.

The timing of maximum monthly total (wildfire and deforestation) fire carbon emissions are shown in Fig. 6 compared to values reported in GFEDv2 (van der Werf et al., 2006), GICC (Mieville et al., 2010) and RETRO (Schultz et al., 2008). The simulated peaks in monthly mean total carbon emissions occur in the northern high latitude regions in July and August in agreement with the satellite based fire products. For Central America and South East Asia the simulations show maximum monthly values around March-April which also corresponds to the fire products. For the African continent, emissions from high fire regions of the Northern Hemisphere (0–10 °N) peak in February-March. Here GFEDv2 and RETRO show an earlier peak around December-January, whereas the ATSR based GICC product peaks mainly around February. An analysis of the individual driving factors used in the Arora and Boer (2005) algorithm (moisture, biomass and ignition probability) revealed that the seasonality in the simulated fire carbon emissions is largely controlled by the moisture probability (not shown).

5 20th century trends of fire carbon emissions

Figure 10 shows the simulated timeseries using decadal mean total (wildfire and deforestation) fire carbon emissions for different regions for the 20 th century compared to decadal mean estimates reported in GICChist (Mieville et al., 2010). In order to understand the simulated trend, we performed a set of sensitivity experiments to disentangle the importance of the individual external forcing factor: climate, population density, land use change, and wood harvest. Figure 10 also summarizes the results from these sensitivity experiments as percentage changes in decadal mean total fire

carbon loss caused by the individual forcing factors. Before we present the simulated trend in Sect. 5.2 a more detailed analysis of the sensitivity experiments is given in the following Sect. 5.1.

5.1 Sensitivity to external forcing

The sensitivity studies were solely performed with CLM-CN using the fire algorithm based on Arora and Boer (2005), which lead to the best agreement between simulation and contemporary satellite based burned area estimates. Note here, that the fire-carbon system is highly non-linear and therefore the individual sensitivities are not additive. Also, we did not perform sensitivity experiments to evaluate the impact of changing CO_2 concentration and nitrogen deposition on fire carbon emissions.

5.1.1 Climate

To demonstrate the sensitivity of simulated burned area and total (wildfire and deforestation) fire carbon emissions to changes in climate we performed one simulation (AB-CLIM) in which CLM-CN was forced for the years 1973–2004 with the NCEP-NCAR 25 year repeat cycle (1942–1972) unlike the simulation (AB-FULL) which was forced from 1973 onwards with NCEP-NCAR reanalysis data in correspondence to the simulation year (1973–2004).

Figure 7 shows the simulated differences averaged over the period 1973–1997 in annual burned area and total fire carbon emissions together with the changes in the driving factors, precipitation and temperature, as well as with the biomass probability and moisture probability as used in the Arora and Boer (2005) fire algorithm (see Appendix A2). Land surface temperatures averaged over 1973–1997 were higher than the 1948–1972 mean in most regions. The global annual mean land surface temperature increased by 0.3°C. Precipitation changes are much more inhomogeneous, with stronger decreases in precipitation over Central Africa and South East Asia and increases in the USA and parts of South America. The annual burned area corre-

sponds to changes in climate with an increase most pronounced over Central Africa and parts of Southern Europe and decreases in South America, USA and South East Asia. Global annual mean burned area increases by 4 Mha (~2%), and total fire carbon emissions by 0.01 Pg C/year (~1%). Changes in carbon loss are similar to the area burned response pattern. The annual burned area increases over Central Africa and Southern Europe as a direct response to a decrease in precipitation and an enhanced moisture probability. Decreases in the moisture probability lead to a decrease in the burned area in South America and in the eastern US. However, small regions along the US West Coast show a higher annual burned area despite a reduced moisture probability. This increase can be explained by an increase in biomass available for burning and an enhanced biomass probability.

5.1.2 Population density

Besides lightning, humans constitute an important ignition source (Robin et al., 2006), but also actively suppress fires in more densely populated areas in which high property values are typically at risk (Stocks et al., 2003; Theobald and Romme, 2007). Human ignition as well as active fire suppression largely depends on cultural, economic, and other factors. As a result the dynamics of these interactions with respect to wildland fire are difficult to quantify and predict at a regional to global scale (Bowman et al., 2009; Guyette et al., 2002). In this study we made an attempt to parametrize the human ignition probability as a function of population density. Details on how we parametrize the human impact on ignition and fire suppression can be found in the Appendix A4.

Figure 8a shows the difference in total (wildfire and deforestation) fire carbon emissions caused by changing population density from 1850 onwards together with the population density (Fig. 8b) for the dominant fire carbon emissions source regions (Africa, South America, equatorial Asia) and globally. When we do not account for fire suppression, the increase in population density leads to an increase in global total fire carbon emissions of around 30% in the 1990s. All world regions show an increase, which is most pronounced in Southern Hemisphere South America (100%) and equatorial Asia

(70%). Little impact is found for Europe (8%) and boreal Asia (5%).

In contrast, including fire suppression leads to almost no change in global total fire carbon emissions, but to large regional inhomogeneities. Regions such as Europe, Central Asia, South East Asia and Middle East show a strong decrease in total fire carbon emissions (−30, −31, −40, −23% in the 1990s, respectively) as a result of increasing urbanization going along with our assumption of stronger fire suppression efforts in densely populated areas. Overall this leads to a better agreement between simulated fire carbon emissions and the satellite based fire products compared to the simulations that assume a constant human ignition probability (AB-FULL) or only take into account human ignition as a function of population density and not fire suppression (AB-HI), as discussed in Sect. 4.1 and Fig. 4. Other regions are still dominated by the increase in human ignition probability caused by the increase in population density and do not significantly experience a strong fire suppression effect, for example Southern Hemisphere South America, boreal North America and Australia (+15, +10, +20% in the 1990s, respectively).

5.1.3 Land use change and wood harvest

Land use change and wood harvest impact fire carbon emissions by introducing a fire source (deforestation fires, which are frequently used to eliminate biomass in preparation for agricultural use) and by removing biomass available for burning. Thus, the net effect of land use activities can theoretically be either an increase or decrease of fire emissions.

The globally averaged trends in deforestation fire carbon emissions show a large increase over the 20th century (Fig. 9). Largest contributions stem from Asia, Africa and South America for the 1990s. Maximum deforestation fires for the 20th century are simulated in the 1950s and are driven by large land cover changes globally. At the beginning of the 20th century North America, Asia, and Europe are the main contributors to the global deforestation fire flux and Africa and South America are only of minor importance.

Globally the deforestation fire carbon loss in the 1990s equals 141 Tg C/year. However, adding in deforestation and wood harvest reduces the carbon loss from wildfires by 433 Tg C/year (−16%, Fig. 8c). This decrease is explained by a globally reduced biomass caused by land use change and wood harvest. The total fire (wildfire and deforestation) is consequently reduced by 292 Tg C/year (−11%, Fig. 8c).

Regionally, the reduction in total carbon fire emissions is strongest in boreal North America (−21% in the 1960s), temperate North America (−30% in the 1980s), Europe (−25% in the 1990s) and South East Asia (−25% in the 1990s). A few regions and time periods show significantly enhanced total fire carbon emissions, i.e. deforestation fire carbon emissions compensate any given decrease in wildfire emissions caused by reduced biomass availability, such as: boreal North America (1850s to 1920s: 11–44%); temperate North America (1850s to 1890s: 6–15%); Europe (1850s to 1910: 4–11%); boreal Asia (1850s to 1990s: 8–100%); central East Asia (1850s to 1980s: 2–27%) and equatorial Asia (1990s: 13%).

Land use change and wood harvest overall lead to a 24 Pg C reduction in carbon emitted by wildfires between 1850 and 2000, which is partly compensated by deforestation fire carbon emissions of 14 Pg C. Wood harvest accumulates 75 Pg C within the same time period, which is redistributed in wood and paper products. 21 Pg C are gained by the wood and paper product pools through land use change and 42 Pg C are lost to the atmosphere by direct conversion.

Overall land use change activities lead to a net terrestrial carbon source of 1.23 Pg C/year, which is in the range of current estimates ranging between −0.6 Pg C/year and 1.8 Pg C/year (Ito et al., 2008) and in line with a recent estimate of 1.1 to 1.3 Pg C/year by Shevliakova et al. (2009). During 2000–2004 this source decreases to 0.85 Pg C/year. Deforestation fires contribute around 11% to this net carbon source.

5.2 Trend in fire carbon emissions

Mieville et al. (2010) use historical burned area estimates by Mouillot et al. (2006) to

scale contemporary satellite based observations back in time (GICChist). Mouillot et al. (2006) note that for the fire history of the 20th century the underlying data source is too sparse to support a reconstruction with high quantitative accuracy, but should be rather used to identify broad trends and patterns. Here we compare our simulated values against GICChist normalized to the mean state 1900–2000 in Fig. 10, which also summarizes the results from the sensitivity experiments as percentage changes in decadal mean total fire carbon emissions caused by the individual forcing factors (as described in Sect. 5.1).

The trend analysis of our simulation for the 20th century is limited as we only force the model with reanalysis data corresponding to the simulation year from 1948 onwards (before 1948 the model is forced with cyclic 25 years (1948–1972) NCEP/NCAR forcing). Changes in total fire carbon emissions before 1948 are therefore only driven by changes in the external forcing factors: population density, atmospheric CO_2 concentration, nitrogen deposition, land use change, and wood harvest. From 1948 onwards the trend is caused by the full set of external forcings including climate.

Globally we simulate a slight downward trend from 1900 to 1960 in agreement with GICChist, except in the simulation that assumes that human ignition increases with population density, which leads to a moderate upward trend. The last three decades are for all simulations characterized by an upward trend caused by climate variations and large burning events in 1997–1998 caused by ENSO induced droughts.

GICChist shows a decreasing trend over the 20th century in boreal regions and an exponential increase in tropical forests, which the authors relate to more stringent fire suppression policies in boreal regions and the use of fire in deforestation in the tropical regions, respectively. Near the end of the 20th century, they find some evidence of an increase in the burned area of temperate forests.

Our simulated trend agrees with these findings for the boreal zone of North America, although our increase starts slightly later. In particular, land use change leads to deforestation fires between 1900 and 1925 and an increase in total fire carbon emissions. Between 1950–1975, however, wood harvest leads to a reduction in available

biomass and a corresponding decrease in total fire carbon emissions. Overall, this leads to a decreasing trend of total fire carbon emissions. The change over time is much smaller than the one reported in GICChist. The subsequent increase in the simulated fire carbon emissions from 1975 to 2000 is mainly governed by a combination of land use change activities and climate. In contrast, simulation T-FULL shows no trend for the boreal regions over the 20th century.

For South America GICChist shows an increase throughout the 20th century, which is most pronounced in the last three decades. The simulations rather show a large decadal variability in fire carbon emissions, due to variations in the 25 year cyclic climate forcing up to the 1960s followed by a sharp decrease caused by enhanced precipitation rates. Fire carbon emissions then return to higher values during 1970 to 2000.

For Europe our simulations show qualitative agreement with GICChist, but the simulated trends are smaller. The best agreement is achieved by the inclusion over fire suppression. However, in South East Asia the inclusion of fire suppression leads to a pronounced decrease in simulated total fire carbon emissions throughout the 20th century, which is not reported in GICChist.

Africa shows a pronounced upward trend in total fire carbon emissions for the last decades in the 20th century in the simulations as well as in the trend reported by GICChist. In the simulations this trend is explained by a change in climate leading to drier conditions over Northern Hemisphere Africa in the end of the 20th century.

These results are in contrast to the one reported in Ito and Penner (2005). Ito and Penner (2005) constructed an inventory of biomass burning BC and POM emissions for the period 1870–2000 based on a bottom up inventory for open vegetation burning scaled by a top-down estimate for the year 2000. Monthly and interannual variations are derived from TOMS AI between 1979 and 2000. Prior to 1979, emissions are scaled to a CH_4 emission inventory based on land use change (Stern and Kaufmann, 1996). As a result of increasing deforestation rates (Houghton et al., 1983) open vegetation burning increases between 1870 and 2000. This is in contrast to our simulated

decreasing trend in global fire carbon emissions between the 1900s and 1960s caused by strong wood harvest rates and decreases in biomass available for burning. Marlon et al. (2008) compiled sedimentary charcoal records over the last two millennia. Their analysis shows a long-term downward trend in biomass burning between 1–1750 followed by a sharp increase from 1750 to the late 19th century and a decrease from the late 19th to mid-to-late 20th century on the global scale. They hypothesize that the long-term downward trend following 1870 can be explained by land use change and wood harvest, which they argue results in landscape fragmentation and generally less flammable landscapes in many regions. This is qualitatively supported by our results.

Schultz et al. (2008) utilize different satellite products for contemporary fire carbon emissions estimates and an extensive literature review in combination with a numerical fire model to scale these back in time for the time period 1960–2000. In Fig. 11 we compare the annual total carbon emissions as simulated globally to these values. The comparison shows in general a good agreement. Our simulations show a moderate upward trend in total fire carbon emissions between 1970–2000, which is in accordance with RETRO mainly caused by large burning events in 1982–1983 and 1997–1998 associated with the ENSO induced drought conditions. From 1960 to 1970 the simulations show a downward trend, whereas RETRO shows almost no trend. The simulated trend is driven mainly by changes in climate. Other external forcings such as population density, land use change and wood harvest impact only slightly the total carbon emissions between 1960 and 2000 (cf. Fig. 8). This agrees qualitatively with the findings reported in Duncan et al. (2003), who estimated seasonal and interannual variations of CO emission from biomass burning for the period 1979 to 2000 using fire count data from ATSR and AVHRR for seasonal variations and TOM aerosol index as a surrogate to estimate the interannual variability. In their analysis they found an upward trend over the two decades, which was solely related to large burning events in 1997–1998.

6 Discussion and conclusion

In this study we evaluate a new fire algorithm applied in the Community Land Model (CLM-CN, Thornton et al., 2007) and simulate the carbon emissions of fires over the last century. CLM-CN includes a prognostic treatment of fires based on the work by Thonicke et al. (2001). Here we develop a new fire algorithm based on the work by Arora and Boer (2005). Our goal is to reproduce contemporary observed burned areas and fire carbon emissions. For this purpose we extended the model by an explicit treatment of the human ignition and fire suppression as a function of population density. In addition, we introduced a parametrization of deforestation fire carbon emissions making use of land use change transition scenarios (Hurtt et al., 2006). We performed several sensitivity experiments in order to disentangle the effects of external driving factors (population density, land use change and wood harvest, climate) on total fire carbon emissions over the last century. The results of this study allow us to have a self-consistent emission dataset for fire emissions of carbon dioxide, reactive gases and aerosols for the 20th century (not discussed here), which can be applied in chemical transport and climate models.

The new model is able to capture much of the observed mean and variability in burned area and carbon emissions. Simulated global annual total fire carbon emissions range between 2.0 and 2.4 Pg C/year for the time period 1997 to 2004, which is within the uncertainty of satellite based fire product estimates. For the most part the model captures the observationally based estimates for the distribution of fires, but we consistently find an overestimation in annual area burned and fire carbon emissions for South America and an underestimation for Africa when we compare our simulations to a range of observations. This mismatch could be the result of several factors including an overestimation of the live aboveground biomass in the Amazon basin in CLM-CN (Randerson et al., 2009). For the interannual variability we find a good agreement between simulated total fire carbon emissions and satellite based results. All simulations capture the large interannual variability associated with El-Niño induced drought con-

ditions in equatorial Asia. The seasonal variation reported by satellite based products is reasonably well simulated in the model. However, for Central Africa all simulations tend to simulate the timing of maximum monthly emissions in February to March, which lags about one to two month compared to satellite based estimates. Overall we find the best agreement in terms of spatial variations, interannual and seasonal variability and regional trends simulated over the 20th century for the model configuration CLM-CN using the Arora and Boer (2005) fire algorithm extended by a parametrization of human ignition and fire suppression as a function of population density when compared to contemporary satellite based fire products and historical records.

In order to improve the fire model, and generally our understanding of fires in the Earth System, we require improved data on a global scale. Large discrepancies remain between the different satellite sensor products (Boschetti et al., 2004; Roy and Boschetti, 2009; Chang and Song, 2009), which hampers the validation in many regions. Improved satellite fire products advanced by uncertainty ranges would greatly enhance the further improvement and development of global fire algorithms. Also, estimates of deforestation fire carbon emissions are associated with large uncertainties. In our model they depend strongly on the assumptions made in the underlying land use change scenario, wood harvest rates and the apportionment of carbon affected by land use change into the single product and conversion pools. In addition, the breakdown of the conversion flux into fire and non-fire related carbon emissions using ratios that solely depend on the moisture driven fire probability, as done in this study, does not account for cultural and socio-economic factors that often control deforestation fire emissions (Morton et al., 2006; Geist, 2001). Satellite based estimates on forest clearing (Hansen et al., 2008) combined with satellite based fire products should improve our understanding of deforestation fires in the future and will help to further improve the deforestation fire parametrization introduced in this study. In addition, there are many important processes related to fires that are not included in the fire algorithms used in this study such as maintenance fires (van der Werf et al., 2009), seasonal changes in combustion factors due to varying fuel moisture and litter amounts (Hoffa et al., 1999),

and peat fires (Page et al., 2002). Also, a more detailed analysis of the relationship between population distribution and human ignition and fire suppression is an important task to reduce uncertainties in the modelling of fires.

Using the model we predict the following results for the trend of fire emissions during the 20th century:

- The simulations show a small global downward trend in decadal mean fire carbon emissions between 1900 and 1960 (∼−5%). This downward trend is in many regions explained by land use change and wood harvest and an associated decrease in available biomass.
- The last three decades in the 20th century are dominated by an upward trend in global total fire carbon emissions (∼+30%) caused by climate variations and large burning events associated with ENSO induced drought conditions.
- Land use change activities between 1850 and 2000 lead to simulated total carbon emissions from deforestation fires of 14 Pg C, but reduced carbon emissions from wildfires by 24 Pg C. Thus, total (wildfire and deforestation) fire carbon emissions are reduced by 10 Pg C (−3%).
- The net flux of carbon to the atmosphere due to land use activities is simulated as 1.2 Pg C/year for 1990–1999 (similar to previous estimates in Ito et al., 2008; Shevliakova et al., 2009). For 2000–2004 this source decreases to 0.85 Pg C/year. 11% of this source is in the model attributed to deforestation fires.
- The simulated deforestation fires contribute about 6–9% to the total global fire carbon emissions for 1990–1999. Largest contribution (8–15%) is simulated in the 1950s due to strong land use change activities globally.

Our 20th century trends are generally in line with estimates based on sedimentary charcoal records (Marlon et al., 2008) and historical estimates based on published

data, land use practices, qualitative reports and tree ring analysis (Mouillot et al., 2006). However, discrepancies remain on regional scales and further work is required to resolve these differences.

Although the model is limited in the processes considered and simplified in many aspects, it captures reasonably well the global distribution and interannual variability of such a complex process as fire carbon emissions and allows further studies assessing the impact of changes in external forcings on past and future fires. When introduced into an Earth system model, this model can build the framework to quantify fire-climate feedbacks in the past and future.

Appendix A

Fire algorithms in CLM-CN

Two fire algorithms are implemented into CLM-CN based on the work by Thonicke et al. (2001) and Arora and Boer (2005). The fire algorithms have in common, that they first estimate the area burned and then carbon fluxes related to combustion and mortality. While Thonicke et al. (2001) uses an empirical relationship relating fire season length and burned area, Arora and Boer (2005) introduces a process based fire parametrization. Both algorithms and their implementation into CLM-CN are described more in detail in the following sections.

A1 Fire algorithm based on Thonicke et al. (2001)

The fire algorithm developed for the LPJ model (Sitch et al., 2003) is modified to translate from the original annual time step to the sub-daily time step used for carbon and nitrogen calculations in CLM-CN. The algorithm assumes that fire occurrence is solely a function of fuel-availability and inferred fuel moisture conditions. Ignition sources are assumed to be ubiquitous. Details on the assumptions made can be found in Thonicke

et al. (2001). Here it is reported how the algorithm is implemented into CLM-CN.

A1.1 Fire probability

A minimum of 100 g C/m^2 of dead fuel is required for fire occurrence. The dead fuel density in CLM-CN is the sum of the litter and coarse woody debris pool. In order to allow fire occurrence and fire spread the fuel moisture has to be below a certain threshold (moisture of extinction, m_e). The moisture of extinction is assumed to be 0.3 for woody biomass and 0.2 for herbaceous biomass. As a substitute for fuel moisture, which is not simulated in CLM-CN, the soil moisture (m) as a fraction of the plant-available volumetric water content of the top 5 cm of the soil column is used similar to Thonicke et al. (2001). In addition to fuel availability and fuel moisture constraints fire occurrence is controlled by surface temperatures, which has to be above freezing.

The probability of fire occurrence at least once a day is given as:

$$\mathrm{fp} = \begin{cases} \exp\left(-\pi * \left(\frac{m}{m_e}\right)^2\right) & \text{if fuel density} > 100\,\mathrm{g\,C/m^2}, \\ & m < m_e, \\ & \text{and } T > 273.15\,\mathrm{K}, \\ 0 & \text{otherwise}. \end{cases} \quad \text{(A1)}$$

A1.2 Area burned

In Thonicke et al. (2001) the daily fire occurrence probability is used to estimate the annual mean fire season length (N, [days/yr]), by summing fp over a year, with N updated once a year. In CLM-CN this is modified. N is updated every model timestep using an e-folding approximation for the annual sum of fp. This translates the annual time step from Thonicke et al. (2001) into the sub-daily model timestep of CLM-CN to account for seasonal variations in fire occurrence.

The e-folding approximation is done as follows: The n-time step running mean of a variable x at the model time step i ($\bar{x}_i$) is approximated by the following weighted

sum:

$$\bar{x}_i = \bar{x}_{i-1}\frac{n-1}{n} + x_i\frac{1}{n} \quad \text{(A2)}$$

For an annual running mean the number of e-folding timesteps (n) is set to the number of model time steps in a year.

Following Thonicke et al. (2001) the annual fractional area burned (f_{annual}, [fraction burned/yr]) is derived from the one-year e-folding mean fire probability ($\bar{\text{fp}}_i$) at each model timestep i:

$$f_{\text{annual}} = \bar{\text{fp}}_i * \exp\left(\frac{s-1}{0.45(s-1)^3 + 2.83(s-1)^2 + 2.91(s-1) + 1.04}\right) \quad \text{(A3)}$$

The fractional area burned per time step in seconds Δt ($f_{\Delta t}$) is given as:

$$f_{\Delta t} = \begin{cases} \frac{\text{fp}_i}{N} f_{\text{annual}} \frac{\Delta t}{86400} & \text{for } N = 365 * \bar{\text{fp}}_i \neq 0, \\ 0 & \text{for } N = 365 * \bar{\text{fp}}_i = 0. \end{cases} \quad \text{(A4)}$$

A2 Fire algorithm based on Arora and Boer (2005)

The fire algorithm developed for the CTEM model (Verseghy et al., 1993) is implemented into CLM-CN. Details on the algorithm are given in Arora and Boer (2005). Here it is reported how the algorithm is implemented into CLM-CN.

A2.1 Fire probability

Total probability of fire occurrence is estimated as the product of three scalars that represent control from biomass, moisture and ignition:

$$P = P_{\text{b}} P_{\text{m}} P_{\text{i}} \quad \text{(A5)}$$

where P_b takes into account that a certain biomass has to be available for burning and is represented as:

$$P_{\text{b}} = \max[0, \min(1, (F - F_l)/(F_u - F_l))] \quad \text{(A6)}$$

with F_l=200 g C/m^2 and F_u=1000 g C/m^2 and F is the aboveground biomass available for burning (combined leaf, stem, litter and coarse woody debris (cwd) pools over all PFTs).

P_m is the fire probability conditioned on the moisture (m) and expressed as follows:

$$P_m = 1 - \tanh(1.75 * m/m_e)^2 \quad \text{(A7)}$$

m_e is the moisture of extinction, defined here as 0.35 independent of fuel type. We defined m in the same way as for the Thonicke et al. (2001) algorithm as a fraction of plant-available volumetric water content in the top 5 cm of the soil as a surrogate for fuel moisture content.

P_i represents the probability of an ignition source, which can be either human or natural (lightning). Ignition due to lightning is represented using cloud to ground lightning frequency (flashes/km^2/month) which is linearly scaled between essentially no flashes (LF_{low}=0.02 flashes/km^2/month) and the maximum observed values (LF_{up}=0.70 flashes/km^2/month).

$$\beta_i = \max[0, \min(1, (LF - LF_{low})/(LF_{up} - LF_{low}))] \quad \text{(A8)}$$

For the lightning frequency we used the Lightning Imaging Sensor/Optical Transient Detector product (LIS/OTD, 2010) which reports total flash rates (cloud-to-ground and intracloud flashes). We estimated the fraction of the total flash rate that can ignite a fire (cloud-to-ground flashes) by introducing a latitude dependency of the fraction of total flashes to cloud-to-ground flashes (Pierce, 1969).

The probability of the ignition by lightning is formulated as follows:

$$P_l = \beta_i/(\beta_i + \exp(1.5 - 6\beta_i)) \quad \text{(A9)}$$

The total ignition potential (combination of natural ignition and human potential (P_h)) is formulated according to:

$$P_i = P_l + (1 - P_l)P_h \quad \text{(A10)}$$

A2.2 Area burned

The area burned is assumed to form an elliptical shape around the point of ignition defined by the fire spread rates in upwind and downwind directions as well as the length-to-breath ratio of the ellipse. To be in accordance with the daily time step used in Arora and Boer (2005) we apply an e-folding approximation of the daily mean following Eq. (A2). For the area burned calculations we exactly use the formulation given by Arora and Boer (2005). For completeness we report them here. For details on the parameters and assumptions applied we refer the reader to Arora and Boer (2005). The fire spread rate in [km/h] in downwind direction is represented as:

$$u_p = g(\mathrm{ws})h(m)u_{\max} \tag{A11}$$

with $u_{\max}$ the maximum fire spread rate (0.45 km/h).

The dependence on the wind speed is given by

$$g(\mathrm{ws}) = 1.0 - (1.0 - g_0)\exp(-(\mathrm{ws}^2/2500)) \tag{A12}$$

In here g_0 is 0.1 and ws is the wind speed in [km/h].

The dependence upon the moisture is represented with $h(m)$

$$h_m = (1 - \beta_m)^2 \tag{A13}$$

$$\beta_m = \begin{cases} m/m_{\mathrm{e}} & \text{for } m < m_{\mathrm{e}}, \\ 1 & \text{for } m > m_{\mathrm{e}}. \end{cases} \tag{A14}$$

The length to breath ratio is given by:

$$l_{\mathrm{b}} = 1 + 10(1 - \exp(-0.017 * \mathrm{ws})) \tag{A15}$$

Assuming that the downwind fire spread rate equals 0.2 the upwind fire spread rate, the total area burned in [km^2] is then given as:

$$a = 0.36 * \pi * u_p^2 / l_{\mathrm{b}} * t^2 \tag{A16}$$

BGD
7, 565–630, 2010

Assuming that the fire burns on average one day, the actual potential area burned within one day can be approximated as:

$$A = a\,(1-q)(2-q)/q^2 \tag{A17}$$

with q=0.5. The area affected in a time step is then given as the product of fire probability (P), the potential area burned (A) divided by the number of model timesteps within a day ($86\,400/\Delta t$)

$$A_{\text{burn}} = A * P * (\Delta t/86\,400) \tag{A18}$$

This area burned (A_{burn}) is according to Arora and Boer (2005) representative for 1000 km^2. The fractional area burned per time step Δt is subsequently given by:

$$f_{\Delta t} = A_{\text{burn}}/1000. \tag{A19}$$

A3 Fire emission, combustion completeness and mortality

To account for different levels of mortality associated with fire in different vegetation types and that only part of the affected biomass is combusted and released into the atmosphere, we introduce a mortality factor (mort) and a combustion completeness factor (cc) as functions of the different PFTs and fuel types considered in CLM-CN. Similar factors are defined by Arora and Boer (2005). Thonicke et al. (2001) only uses a "fire resistance" factor (1−mort), which varies among different plant functional types, but does not account for the fact that biomass is only partly combusted during a fire. In CLM-CN we modified the Thonicke et al. (2001) algorithm by adding a woody combustion completeness factor (0.2) that is applied to all woody fuel types. All other fuel types are completely combusted. Values for mort and cc are given in Tables A1 and A2.

The amount of carbon released into the atmosphere for each PFT is given as:

$$E_{\text{PFT}} = f_{\Delta t} \cdot C \cdot \text{cc} \cdot \text{mort} \tag{A20}$$

with $C=(C_{\text{leaf}}, C_{\text{stem}}, C_{\text{root}}, C_{\text{litter}}, C_{\text{cwd}})$ being a vector of carbon concentrations in [g/m^2] for the different fuel types considered in CLM-CN and cc and mort being a vector of combustion completeness and mortality factors, respectively, as defined in Tables A1 and A2. The amount of carbon killed during a fire and transferred to the litter pool for each PFT is given as:

$$T_{\text{PFT}} = f_{\Delta t} C (1 - \text{cc}) \text{mort} \quad \text{(A21)}$$

Total carbon emission (E_{c}) are given as the area weighted sum over all PFTs. The same applies for nitrogen.

A4 Human influence

Humans influence fires by ignition (intentionally or accidentally) and at the same time they impact fires actively by fire suppression. To account for these effects we introduce a parametrization of the human ignition potential and fire suppression as a function of population density. Population density data are taken from the HYDE dataset for the years 1850–2000 (Klein Goldewijk, 2001).

In an initial attempt the probability for human fire ignitions is assumed to be constant globally (0.5) as done in Arora and Boer (2005). To account more explicitly for human ignition probability we use the relationship given by Venesky et al. (2002) relating fire danger to population density (popd) in terms of interactions of humans with natural ecosystems (Fire danger $=6.8 * \text{popd}^{-0.57}$). This relationship assumes that an average person is more likely to cause a fire in sparsely populated regions, as they interact more with the natural ecosystems compared to persons living in densely populated areas. For densely populated regions we apply a lower threshold of 300 inhabitants/km^2 (pd_{up}). The human ignition probability is then given by:

$$P_{\text{h}} = \min\left(1, \text{popd} * 6.8 * \text{popd}^{-0.57} / \left(\text{pd}_{\text{up}} * 6.8 * \text{pd}_{\text{up}}^{-0.57}\right)\right) \quad \text{(A22)}$$

Fire suppression will also depend on the population density. Fire suppression will more likely take place in densely populated areas were typically high property values are at

risk compared to sparsely populated areas (Stocks et al., 2003; Theobald and Romme, 2007). We parametrize fire suppression similar to Pechony and Shindell (2009) as follows:

$$F_{\text{supp}} = 1. - (0.10 + \exp(-0.025 * \text{popd})) \quad \text{(A23)}$$

assuming that in more densely populated areas 90% of the fires will be suppressed. Fire suppression will impact natural (lightning induced) fires as well as human initiated fires. The total ignition probability is then given as:

$$P_{\text{i}} = (P_{\text{l}} + (1 - P_{\text{l}}) * P_{\text{h}}) * (1. - F_{\text{supp}}) \quad \text{(A24)}$$

Figure A1 illustrates the human ignition probability as a function of population density. Unsuppressed human ignitions peak around 10–20 inhabitants/km^2 which is in agreement with the analysis performed by Barbosa et al. (1999) for Africa.

A5 Deforestation fires

To account for deforestation fires in CLM-CN we modified the current treatment of dynamic land cover within CLM-CN. Changes in land cover area over time are prescribed from an external dataset following the annual land cover change given by Hurtt et al. (2006) for the time period 1850–2004. Land cover change is given by an annual time-series of globally gridded information about the subgrid fractional area occupied by the single plant functional types (PFTs) within a grid-cell. The annual rate is equally distributed across the number of timesteps simulated in CLM-CN within a year. For the case that land cover change leads to a reduction of the area occupied by a single PFT, the associated carbon and nitrogen loss is distributed into a wood production pool, paper production pool and a conversion flux. The relative rates for this redistribution are given in Table A3.

For the wood product pool a residence time of 100 years is assumed, for the paper production pool 10 years and the conversion flux is released immediately into the at-

mosphere. The conversion flux has a fire component in many regions that experience favourable burning conditions.

We modified the CLM-CN scheme to account for the fraction of the conversion flux which will be likely fire driven (deforestation fires) as follows:

The conversion flux is divided into a fire and non-fire related pool. For this we define a fire-scalar (fs) as a function of the annual mean fire moisture probability ($P_{\mathrm{m,annual}}$) simulated within the fire algorithm in CLM-CN (see Eqs. A1 and A7, respectively).

We assume that in regions with a high annual mean fire moisture probability, land managers will more likely burn forest biomass during the land clearing process. The fire-scalar is given as:

$$\mathrm{fs} = \mathrm{fs}_{\mathrm{min}} + (\max[0, \min(1, (P_{\mathrm{m,annual}} - \mathrm{fa}_{\mathrm{low}})/(\mathrm{fa}_{\mathrm{high}} - \mathrm{fa}_{\mathrm{low}}))]) * (\mathrm{fs}_{\mathrm{max}} - f s_{\mathrm{min}})$$

In an initial attempt we assume that the maximum and minimum fraction of the conversion flux ($\mathrm{fs}_{\mathrm{min}}$) and ($\mathrm{fs}_{\mathrm{max}}$) that is redirected to the fire and non-fire pool are constant globally (0.2 and 0.8, respectively). However, this ratio will also largely depend on cultural practices and is therefore likely to vary for different regions and different time periods.

Low and high annual mean moisture fire probabilities ($\mathrm{fp}_{\mathrm{low}}$) and ($\mathrm{fp}_{\mathrm{high}}$) are set to 0.01 and 0.30, respectively. Annual mean moisture fire probabilities are below 0.01 for example in wet regions like northern Europe and the east coast of the USA, whereas values larger than 0.30 are simulated only in very dry regions such as Central Africa and Australia. Annual mean fire probabilities slightly differ between the two fire-algorithms applied in this study. However, we use the same thresholds for both.

The flux into the fire pool and non-fire pool is given as:

$$\mathrm{fire\_pool}_{\mathrm{gain}} = \mathrm{CONV} * \mathrm{fs} \quad \text{(A25)}$$

$$\mathrm{non\_fire\_pool}_{\mathrm{gain}} = \mathrm{CONV} * (1 - \mathrm{fs}) \quad \text{(A26)}$$

with CONV being the carbon and nitrogen mass flux attributed to the conversion flux.

The flux out of the fire-pool follows a rate constant, which is a function of the instantaneous moisture fire probability ($p_{m,inst}$) as simulated within the fire-algorithm. Carbon in the fire-pool can accumulate over a certain time-period (τ_{max}) in which conditions are relatively wet and is only released into the atmosphere when conditions get sufficiently dry (Morton et al., 2008; van der Werf et al., 2009). The rate constant which controls the flux out of the fire pool is given as:

$$\tau_{fire} = \tau_{min} + \max[0, \min(1, (P_{m,inst} - fi_{low})/(fi_{high} - fi_{low}))] * (\tau_{max} - \tau_{min}) \quad \text{(A27)}$$

τ_{min} and τ_{max} are set to give a 90% loss of the initial mass of the fire-pool to be released into the atmosphere within 3 years and 1 week, respectively. fi_{low} and fi_{high} are set to 0.0 and 1.0. The flux out of the non-fire pool into the atmosphere is immediate (fuel wood).

The flux out of the fire pool and non-fire pool is given as:

$$fire\_pool_{loss} = fire\_pool * \tau_{fire} \quad \text{(A28)}$$

$$non\_fire\_pool_{loss} = non\_fire\_pool * 1. \quad \text{(A29)}$$

with fire_pool and non_fire_pool representing the carbon and nitrogen mass in the fire and non-fire pool, respectively.

In addition to land cover change CLM-CN accounts explicitly for changes in wood harvest activity (Hurtt et al., 2006). Wood harvest is solely related to logging and is not directly related to fires. However, wood harvest will alter the biomass available for burning and thus natural fires as well as deforestation fires (see Sect. 5.1.3).

Acknowledgements. This work was supported by NSF-0758369. For computational support the authors acknowledge NSF and NCAR. We thank the participants and organizers of the AIMES workshop "Cultural Uses and Impacts of Fires" as well as S. Harrison, K. Thonicke and G. van der Werf for helpful discussion.

References

Andreae, M., Rosenfeld, D., Artaxo, P., Costa, A., Grank, G., Longo, K., and Silva-Dias, M.: Smoking rain clouds over the amazon, Science, 303, 1337–1342, 2004. 567

Arora, V. and Boer, G.: Fire as an interactive component of dynamic vegetation models, J. Geophys. Res., 110, G02008, doi:10.1029/2005JG000042, 2005. 566, 567, 568, 570, 571, 572, 579, 580, 581, 588, 589, 591, 593, 595, 596, 597, 609, 614

Barbosa, P., Stroppiana, D., Gregoire, J.-M., and Pereira, J.: As assessment of vegetation fire in Africa (1981–1991): Burned areas, burned biomass, and atmospheric emissions, Global Biogeochem. Cy., 13, 933–950, 1999. 598

Bond, W. J., Woodward, F. I., and Midgley, G. F.: The global distribution of ecosystems in a world without fire, New Phytol., 165(2), 525–538, doi:10.1111/j.1469-8137.2004.01252.x, 2004. 567

Boschetti, L., Eva, H., Brivio, P., and Gregoire, J.: Lessons to be learned form the comparison of the three satellite-derived biomass burning products, Geophys. Res. Lett., 31, L21501, doi:10.1029/2004GL021229, 2004. 574, 589

Bowman, D., Balch, J., Artaxo, P., Bond, W., Carlson, J., Cochrane, M., D'antonio, C., De Fires, R. S. ad Doyle, J., Harrison, S., Johnston, F., Keeley, J., Krwchuk, M., Kull, C., Marston, J., Mortiz, M., Prentice, I., Roos, C., Scott, A., Swetnam, T., van der Werf, G., and Pyne, S.: Fire in the Earth system, Science, 324, 481, doi:10.1126/science.1163886, 2009. 567, 582

Chambers, S., Beringer, J., Randerson, J., and Chapin III, F.: Fire effects on net radiation and energy partitioning: Contrasting responses of tundra and boreal forest ecosystems, J. Geophys. Res., 110, D09106, doi:10.1029/2004JD2005299, 2005. 567

Chang, D. and Song, Y.: Comparison of L3JRC and MODIS global burned area products from 2000 to 2007, J. Geophys. Res., 114, D16106, doi:10.1029/2008JD011361, 2009. 574, 576, 589

Crutzen, P., Heidt, L., Krasnec, J., Pollock, W., and Seiler, W.: Biomass burning as a source of atmospheric gases CO,H_2, N_2O, NO, CH_3CL and COS, Nature, 282, 253–256, doi:10.1038/282253a0, 1979. 567

Decker, R. and Zeng, X.: Impact of modified richards equation on global soil moisture simulation in the Community Land Model (CLM3.5), J. Adv. Model. Earth Syst., 1, doi:10.3894/JAMES.2009.1.5, 2009. 569, 570

Duncan, B., Martin, R., Staudt, A., Yevich, R., and Logan, J.: Interannual and seasonal variability of biomass burning emissions constrained by satellite observations, J. Geophys. Res., 108, 4100, doi:10.1029/2002JD002378, 2003. 587
Feingold, G., Remer, L., Ramaprasad, J., and Kaufman, Y.: Analysis of smoke impact on clouds in Brazilian biomass burning regions: An extension of Twomey's approach, J. Geophys. Res., 103, 22907–22922, 2001. 567
Flanner, M. and Zender, C.: Snowpack radiative heating: Influence on Tibetan Plateau climate, J. Geophys. Res., 32, L06501, doi:10.1029/2004GL022076, 2005. 569
Flanner, M. and Zender, C.: Linking snowpack microphysics and albedo evolution, J. Geophys. Res., 111, D12208, doi:10.1029/2005JD006834, 2006. 569
Flanner, M., Zender, C., Randerson, J., and Rasch, P.: Present-day climate forcing and response from black carbon in snow, J. Geophys. Res., 112, D11202, doi:10.1029/2006JD008003, 2007. 569
Geist, H.: What drives tropical deforestation? A meta-analysis of proximate and underlying causes of deforestation based on subnational case study evidence, in: Land-Use and Land-Cover Change (LUCC) Project Report Series, vol. 4, published by: LUCC International Project Office, University of Louvain, Belgium, 2001. 589
Giglio, L., van der Werf, G. R., Randerson, J. T., Collatz, G. J., and Kasibhatla, P.: Global estimation of burned area using MODIS active fire observations, Atmos. Chem. Phys., 6, 957–974, 2006, http://www.atmos-chem-phys.net/6/957/2006/. 567, 573
Glantz, M.: Currents of Change, Impacts of El Nino and La Nina on Climate and Society, Cambridge Univ. Press, New York, 2001. 579
Gregoire, J.-M., Tansey, K., and Silva, J.: The GBA2000 initiative: Developing a global burned area database from SPOT-VEGETATION imagery, Int. J. Remote Sens., 24, 1369–1376, 2002. 573
Guyette, R., Musika, R., and Dey, D.: Dynamics of an anthropogenic fire regime, Ecosystems, 5, 472–486, doi:10.1007/s10021-002-0115-7, 2002. 582
Hansen, M., Sheman, S., Potapov, P., Loveland, T., Townshend, J., DeFries, R., Pittman, K., Arunarwati, B., Stolle, F., Steininger, M., Caroll, M., and DiMiceli, C.: Humid tropical forest clearing from 2000 to 2005 quantified by using multitemporal and multiresolution remotely sensed data, P. Natl. Acad. Sci., 105, 9439–9444, 2008. 589
Hoffa, E. A., Ward, D. E., Hao, W., Susott, R. A., and Wakimoto, R. H.: Seasonality of carbon emissions from biomass burning in a Zambian savanna, J. Geophys. Res., 104, 13841–

13853, 1999. 589
Houghton, R., Hobbie, J., Melillo, J., Morre, B., Pterson, B., Shaver, G., and Woodwell, G.: Changes in the carbon content of terrestial biota and soils between 1860 and 1980 – a net release of CO_2 to the atmosphere, Ecol. Monogr., 53, 235–262, 1983. 586, 615
Hurtt, G., Frolking, S., Fearon, M., Morre, B., Shevliakova, E., Malyshev, S., Pacala, S., and Houghton, R.: The underpinnings of land-use history: three centuries of global gridded land-use transitions, wood harvest activity, and resulting secondary lands, Global Biogeochem. Cy., 12, 1208–1229, doi:10.1111/j.1365-2486.2006.01150.x, 2006. 568, 572, 588, 598, 600, 609
Ito, A. and Penner, J.: Global estimates of biomass burning emissions based on satellite imagery for the year 2000, J. Geophys. Res., 109, D14S05, doi:10.1029/2003JD004423, 2004. 576
Ito, A. and Penner, J.: Historical emissions of carbonaceous aerosols from biomass and fossil fuel burning for the period 1870–2000, Global Biogeochem. Cy., 19, GB2028, 2005. 586
Ito, A., Ito, A., and Akimoto, H.: Seasonal and interannual variations in CO and BC emissions from open biomass burning in Southern Africa during 1998–2005, Global Biogeochem. Cy., 21, GB2011, doi:10.1029/2006GB002848, 2007. 576
Ito, A., Penner, J. E., Prather, M. J., de Campos, C. P., Houghton, R. A., Kato, T., Jain, A. K., Yang, X., Hurtt, G. C., Frolking, S., Fearon, M. G., Chini, L. P., Wang, A., and Price, D. T.: Can we reconcile differences in estimates of carbon fluxes from land-use change and forestry for the 1990s?, Atmos. Chem. Phys., 8, 3291–3310, 2008, http://www.atmos-chem-phys.net/8/3291/2008/. 584, 590
Kasischke, E. and Bruhwiler, L.: Emissions of carbon dioxide, carbon monoxide, and methane from boreal forest fires in 1998, J. Geophys. Res., 108, 461, doi:10.1029/2001JD000, 2003. 579
Kasischke, E. and Penner, J.: Improving global estimates of atmospheric emissions from biomass burning, J. Geophys. Res., 109, D14S01, doi:10.1029/2004JD004972, 2004. 567, 576
Klein Goldewijk, K.: Estimating global land use change over the past 300 years, Global Biogeochem. Cy., 15, 417–433, 2001. 572, 597, 609
Kreidenweis, S., Remer, L., Bruintjes, R., and Dubovik, O.: Smoke aerosol from biomass burning in Mexico: Hygroscopic smoke optical model, J. Geophys. Res., 106, 4831–4844, 2001. 579

Lamarque, J.-F., Kiehl, J. T., Brasseur, G. P., Butler, T., Cameron-Smith, P., Collins, W. D., Collins, W. J., Granier, C., Hauglustaine, D., Hess, P. G., Holland, E. A., Horowitz, L., Lawrence, M. G., McKenna, D., Merilees, P., Prather, M. J., Rasch, P. J., Rotman, D., Shindell, D., and Thornton, P.: Assessing future nitrogen deposition and carbon cycle feedbacks using a multi-model approach: Analysis of nitrogen deposition, J. Geophys. Res., 110, D19303, doi:10.1029/2005JD005825, 2005. 572

Lawrence, D. and Slater, A.: Incoporating organic soil into a global climate model, Clim. Dynam., 30(2–3), 145–160, doi:10.1007/s00382-007-0278-1, 2008a. 569

Lawrence, D. and Slater, A.: The contribution of snow condition trends to future ground climate, Clim. Dynam., doi:10.1007/s00382-009-0537-4, online available at: http://www.springerlink.com/content/ek23345lr125x716/, 2009. 569

Lawrence, D., Slater, A., Roanovsky, V., and Nicolsky, D.: Sensitivity of a model projection of near-surface permafrost degradation to soil column depth and representation of soil organic matter, J. Geophys. Res., 113, F02011, doi:10.1029/2007JF000883, 2008b. 569

Lawrence, P. and Chase, T.: Representing a new MODIS consistent land surface in the Community Land Model (CLM 3.0), J. Geophys. Res., 112, G01023, doi:10.1029/2006JG000168, 2007. 570

Lehsten, V., Tansey, K., Balzter, H., Thonicke, K., Spessa, A., Weber, U., Smith, B., and Arneth, A.: Estimating carbon emissions from African wildfires, Biogeosciences, 6, 349–360, 2009, http://www.biogeosciences.net/6/349/2009/. 575, 578, 610

LIS/OTD: Lightning Imaging Sensor/Optical Transient Detector: NASA LIS/OTD Science Team (Principal Investigator, Dr. Hugh J. Christian, NASA/Marshall Space Flight Center), online available at: http://ghrc.nsstc.nasa.gov/uso/ds_docs/lis_climatology/lohrmc_dataset.html, last acess: January 2010. 594

Liu, H. and Randerson, T.: Interannual variability of surface energy exchange depends on stand age in a boreal forest fire chronosequence, J. Geophys. Res., 113, G01006, doi:10.1029/2007JG000483, 2008. 567

Marlon, J., Bartlein, P., Carcaillet, C., Gavin, D., Higuera, P., Joos, F., Power, M., and Prentice, I.: Climate and human influences on global biomass burning over the past two millennia, Nat. Geosci., 1, 697–702, doi:10.1038/ngeo313, 2008. 574, 587, 590

Mieville, A., Granier, C., Liousse, C., Guillaume, B., Mouillot, F., Lamarque, J., Gregoire, J., and Petron, G.: Emissions of gases and particles from biomass burning during the 20th century using satellite data and a historical reconstruction, online available at: http://www.

aero.jussieu.fr/projet/ACCENT/GICC_metadata.php, in preparation, 2010. 568, 573, 574, 577, 579, 580, 584, 612, 618, 619, 620, 621, 625

Morton, D., DeFries, R., Shimabukuro, Y., L.O., A., Arai, E., del Bon Espirio-Santo, F., Freitas, R., and Morisette, J.: Cropland expansion changes deforestation dynamics in southern Brazil Amazon, P. Natl. Acad. Sci., 103, 14637–14641, 2006. 589

Morton, D., deFries, R., Randerson, J., Giglio, L., Schroeder, W., and van der Werf, G.: Agricultural intensification increases deforestation fire activity in Amazonia, Glob. Change Biol., 14, 2262–2275, 2008. 600

Mouillot, F., Narasimha, A., Balkansji, Y., Lamarque, J.-F., and Field, C. B.: Global carbon emissions from biomass burning in the 20th century, Geophys. Res. Lett., 33, L01801, doi:10.1029/2005GL024707, 2006. 574, 584, 585, 591

Niu, G.-Y. and Yang, Z.-L.: An observation-based formulation of snow cover fraction and its evaluation over large North American river basins, J. Geophys. Res., 112, D21101, doi:10.1029/2007JD008674, 2007. 569

Oleson, K., Niu, G.-Y., Yang, Z.-L., Lawrence, D., Thornton, P., Lawrence, P., Stoeckli, R., Dickinson, R., Bonan, G., Levis, S., Dai, A., and Qian, T.: Improvements to the Community Land Model and their impact on the hydrological cyle., J. Geophys. Res., 113, G01021, doi:10.1029/2007JG000563, 2008a. 569

Oleson, K., Bonan, G., Feddema, J., Vertenstein, M., and Grimmong, C.: An urban parameterization for a global climate model. 1. Formulation and evaluation of two cities, J. Appl. Meteorol. Clim., 47, 1038–1060, 2008b. 569, 570

Page, S., Siegert, F., Rieley, J., Boehm, H.-D. V., Jaya, A., and Limin, S.: The amount of carbon released from peat and forest fires in Indonesia during 1997, Nature, 420, 61–64, 2002. 568, 590

Pechony, O. and Shindell, D.: Fire parameterization on a global scale, J. Geophys. Res., 114, D16115, doi:10.1029/2009JD011927, 2009. 567, 598

Penner, J. E., Dickison, R. E., and O'Neill, C. A.: Effects of aerosol from biomass burning on the global radiation budget, Science, 256, 1432–1434, doi:10.1126/science.256.5062.1432, 1992. 567

Pierce, E.: Latitudinal variation of lightning parameters, J. Appl. Meteorol., 164–165, 1969. 594

Plummer, S., Arino, O., Simon, M., and Steffen, W.: Establishing an earth observation product service for the terrestrial carbon community: the GLOBCARBON initiative, Mitigat. Adapt. Strat. Global Change, 11, 97–111, 2006. 573

Power, M., Marlon, J., Ortiz, N., Bartlein, P., Harrison, S., F.E., M., Ballouche, A., Bradshaw, R., Carcaillet, C., Cordova, C., Mooney, S., Moreno, P., Prentice, I., Thonicke, K., Tinner, W., Whitlock, C., Zhang, Y., Zhao, Y., Ali, A., Anderson, R., Beer, R., Behling, H., Briles, C., Brown, K., Brunelle, A., Bush, M., Camill, P., Chu, G., Clark, J., Colombaroli, D., Connor, S. et al.: Changes in fire regimes since the Last Glacial Maximum: an assessment based on a global synthesis and analysis of charcoal data, Clim. Dynam., 30, 887–907, doi:10.1007/s00382-007-0334-x, 2008. 567

Qian, T., Dai, A., Trenberth, K., and Oleson, K.: Simulation of global land surface conditions from 1948 to 2004. Part I: forcing data and evaluations, J. Hydrometeorol., 7, 953–975, 2006. 568, 572, 609

Ramankutty, N., Evan, A., Monfreda, C., and Foley, J.: Farming the planet. Part 1: the geographic distribution of global agricultural lands in the year 2000, Global Biogeochem. Cy., 22, GB1003, doi:10.1029/2007GB002952, 2008. 570

Randerson, J., Hoffman, F., Thornton, P., Mahowald, N., Lindsay, K., Lee, Y.-H., Nevison, C., Doney, S., Bonan, G., Stoeckli, R., Covey, C., Running, S., and Fung, I.: Systematic assessment of terrestial biogeochemistry in coupled climate-carbon models, Glob. Change Biol., 15, 2462–2484, doi:10.1111/j.1365-2486.2009.01912.x, 2009. 570, 572, 588

Robin, J.-G., Carrega, P., and Fox, D.: Modelling fire ignition in the Alpes-Maritimes Department, France, a comparison, Forest Ecol. Manag., 234, S135, doi:10.1016/j.forecol.2006.08.176, 2006. 568, 582

Roy, D. and Boschetti, L.: Southern Africa validation of the MODIS, L3JRC, and GlobCarbon burned-area products, IEEE Geosci. Remote S., 47(4), 1032–1044, doi:10.1109/TGRS.2008.2009000, 2009. 574, 575, 589

Roy, D., Boschetti, L., Justice, C., and Ju, J.: The Collection 5 MODIS burned area product – global evaluation by comparison with the MODIS active fire product, Remote Sens. Environ., 112, 3690–3707, doi:10.1016/j.rse.2008.05.013, 2008. 573

Sakaguchi, K. and Zeng, X.: Effects of soil wetness, plant litter, and under-canopy atmospheric stability on ground evaporation in the Community Land Model (CLM3.5), J. Geophys. Res., 114, D01107, doi:10.1029/2008JD010834, 2009. 569

Schultz, M., Heil, A., Hoelzemann, J., Spessa, A., Thonicke, K., Goldammer, J., Held, A., Pereira, J., and van het Bolscher, M.: Global wildland fire emissions from 1960 to 2000, Global Biogeochem. Cy., 22, GB2002, doi:10.1029/2007GB003031, 2008. 568, 574, 576, 577, 579, 580, 587, 618, 619, 621, 627

Shevliakova, E., Pacala, S., Malyshev, S., Hurtt, G., Milly, P., Caspersen, J., Sentman, L., Fisk, J., Wirth, C., and Crevoisier, C.: Carbon cycling under 300 years of land use change: importance of the secondary vegetation sink, Global Biogeochem. Cy., 23, GB2022, doi:10.1029/2007GB003176, 2009. 584, 590

Simon, M., Plummer, S., Fierens, F., Hoelzemann, J., and Arino, O.: Burnt area detection at global scale using ATSR-2: The GLOBSCAR products and their qualification, J. Geophys. Res., 109, D14S02, doi:10.1029/2003JD003622, 2004. 573

Sitch, S., Smith, B., Prentice, I., Arneth, A., Bondeau, A., Cramer, W., Kaplan, J., Levis, S., Lucht, W., Sykes, M., Thonicke, K., and Venesky, S.: Evaluation of ecosystem dynamics, plant geography and terrestrial carbon cycling in the LPJ Dynamic Global Vegetation Model, Glob. Change Biol., 9, 161–185, 2003. 570, 591

Smith, B., Prentice, I., and Sykes, M.: Representation of vegetation dynamics in the modelling of terrestial ecosystems: comparing two contrasting approaches within European climate space, Global Ecol. Biogeogr., 10, 621–637, 2001. 578

Soja, A., Cofer, W., Shugart, H., Sukhinin, A., Stackhouse Jr., P., McRae, D., and Conrad, S.: Estimating fire emissions and disparities in boreal Siberia (1998–2002), J. Geophys. Res., 109, D14S06, doi:10.1029/2004JD004570, 2004. 576

Stern, D. and Kaufmann, R.: Estimates of global anthropogenic methane emissions 1860–1993, Chemosphere, 33, 159–176, 1996. 586

Stocks, B., Mason, J., Todd, J., Bosch, E., Wotton, B., Amiro, B., Flannigan, M., Hirsch, K., Logan, K., Martell, L., and Skinner, W.: Large forest fires in Canada, 1959–1997, J. Geophys. Res., 108(D1), 8149, doi:10.1029/2001JD000484, 2003. 568, 582, 598

Stoeckli, R., Lawrence, D., Niu, G.-Y., Oleson, K., Thornton, P., Yang, Z.-L., Bonan, G., Denning, A., and Running, S.: The use of Fluxnet in the Community Land Model development, J. Geophys. Res., 113, G01025, doi:10.1029/2007JG000562, 2008. 569

Tansey, K., Gregoire, J.-M., Defourny, P., Leigh, R., Pekel, J.-F., van Bogaert, E., and Baerholome, E.: A new, global, multi-annual (2000–2007) burnt area product at 1 km resolution, Geophys. Res. Lett., 35, L01401, doi:10.1029/2007GL031567, 2008. 567, 568, 573, 575, 616, 617

Theobald, M. and Romme, W.: Expansian of the US wildland-urban interface, Landscape Urban Plan., 83, 340–354, doi:10.1016/j.landurbplan.2007.06.002, 2007. 582, 598

Thonicke, K., Venesky, S., Sitch, S., and Cramer, W.: The role of fire disturbance for global vegetation dynamics: coupling fire into a Dynamic Global Vegetation Model, Global Ecol.

Biogeogr., 10, 661–667, 2001. 567, 568, 570, 571, 588, 591, 592, 593, 594, 596, 609, 613
Thornton, P. and Rosenbloom, N.: Ecosystem model spin-up: estimating steady state conditions in a coupled terrestial carbon and nitrogen cycle model, Ecol. Model., 189(2), 25–48, 2005. 570
Thornton, P., Law, B., Gholz, H., Clark, K., Falge, E., Ellsworth, D., Goldstein, A., Moson, R., Hollinger, D., Falk, M., Chen, J., and Sparks, J.: Modeling and measuring the effects of disturbance history and climate on carbon and water budgets in evergreen needleleaf forests, Agr. Forest Meteorol., 113, 185–222, 2002. 570
Thornton, P., Lamarque, J., Rosenbloom, N., and Mahowald, N.: Influence of carbon-nitrogen cycle coupling on land model response to CO_2 fertilization and climate variability, Global Biogeochem. Cy., 21, GB4018, doi:10.1029/2006GB002868, 2007. 570, 588
Thornton, P. E., Doney, S. C., Lindsay, K., Moore, J. K., Mahowald, N., Randerson, J. T., Fung, I., Lamarque, J.-F., Feddema, J. J., and Lee, Y.-H.: Carbon-nitrogen interactions regulate climate-carbon cycle feedbacks: results from an atmosphere-ocean general circulation model, Biogeosciences, 6, 2099–2120, 2009, http://www.biogeosciences.net/6/2099/2009/. 568, 570
van der Werf, G. R., Randerson, J. T., Giglio, L., Collatz, G. J., Kasibhatla, P. S., and Arellano Jr., A. F.: Interannual variability in global biomass burning emissions from 1997 to 2004, Atmos. Chem. Phys., 6, 3423–3441, 2006, http://www.atmos-chem-phys.net/6/3423/2006/. 568, 573, 575, 577, 578, 579, 580, 612, 616, 617, 618, 619, 620, 621, 630
van der Werf, G. R., Morton, D. C., DeFries, R. S., Giglio, L., Randerson, J. T., Collatz, G. J., and Kasibhatla, P. S.: Estimates of fire emissions from an active deforestation region in the southern Amazon based on satellite data and biogeochemical modelling, Biogeosciences, 6, 235–249, 2009, http://www.biogeosciences.net/6/235/2009/. 568, 589, 600
Venesky, S., Thonicke, K., Sitch, S., and Cramer, W.: Simulating fire regimes in human-dominated ecosystems: Iberian Peninsula case study, Glob. Change Biol., 8, 984–998, 2002. 571, 597
Verseghy, D., McFarlane, N., and Lazare, M.: CLASS – a Canadian land surface scheme for GCMs: II. Vegetation model and coupled runs, Int. J. Climatol., 13, 347–370, 1993. 570, 593
Wang, A. and Zeng, X.: Improving the treatment of the vertical snow burial fraction over short vegetation in the NCAR CLM3, Adv. Atmos. Sci., 26, 877–886, doi:10.1007/s00376-009-8098-3, 2009. 569

Table 1. Control and transient model simulations analyzed in the present study. Simulations use different fire algorithms, different treatment of human ignition potential, and different assumptions about land-cover change and wood harvest as well as climate forcing.

Name	Fire algorithm[1]	human ignition[2]	pop. density[3]	Land-cover change[4]	CO_2 concentration/[5] Nitrogen deposition	Climate forcing[6]
Control simulations						
C-T	Thonicke	–	–	–	pre-industrial	1948–1972
C-AB	Arora and Boer	constant=0.5	–	–	pre-industrial	1948–1972
C-AB-HI	Arora and Boer	human ignition	pre-industrial	–	pre-industrial	1948–1972
C-AB-HI-FS	Arora and Boer	human ign. and fire suppr.	pre-industrial	–	pre-industrial	1948–1972
Transient simulations: 1798–2004						
T-FULL	Thonicke	–	–	transient	transient	1948–1972/1973–2004
AB-FULL	Arora and Boer	constant=0.5	–	transient	transient	1948–1972/1973–2004
AB-HI	Arora and Boer	human ignition	transient	transient	transient	1948–1972/1973–2004
AB-HI-FS	Arora and Boer	human ign. and fire suppr.	transient	transient	transient	1948–1972/1973–2004
Sensitivity simulations: 1798–2004						
AB-LUC	Arora and Boer	constant=0.5	–	–	transient	1948–1972/1973–2004
AB-CLIM	Arora and Boer	constant=0.5	–	transient	transient	1948–1972
AB-HI-PI	Arora and Boer	human ignition	pre-industrial	transient	transient	1948–1972/1973–2004
AB-HI-FS-PI	Arora and Boer	human ign. and fire suppr.	pre-industrial	transient	transient	1948–1972/1973–2004

[1] Fire algorithm: in CLM-CN based on Thonicke et al. (2001) or Arora and Boer (2005).

[2] different treatment of human ignition: either a constant value of 0.5 (constant), or following a human ignition only (HI) or human ignition and fire suppression scenario (HI-FS).

[3] Population density is considered transient between 1798 and 2004 (Klein Goldewijk, 2001) or held constant at a pre-industrial value (PI),

[4] Land cover change and wood harvest: either no land cover change and wood harvest (–) or transient land cover change and wood harvest between 1850–2004 (Hurtt et al., 2006).

[5] CO_2 concentration and nitrogen deposition are set to pre-industrial values for the control simulations and are transient time-varying for the transient simulations.

[6] Climate forcing: either cycling periodically through NCEP/NCAR data (Qian et al., 2006) for the years 1948–1972 or cycling through 1948–1972 followed by the full time series for the years 1948–2004.

Table 2. Annual mean total (wildfire and deforestation) fire carbon emissions and annual burned areas for Africa (NHAF: Northern Hemisphere Africa, SHAF: Southern Hemisphere Africa) for the different simulations compared to observations. All reported values are averages over the years 2001–2004.

	L3JRC	GFEDv2	Lehsten et al. (2009)*	T-FULL	AB-FULL	AB-HI	AB-HI-FS
area burned [Mha]							
SHAF	87.4±8.0	80.0±3.5	112±15.3	39.0±2.6	74.1±8.0	66.0±7.3	45.45±2.5
NHAF	68.0±7.8	139±10.3	86.7±9.6	19.5±0.5	44.5±2.7	43.8±3.5	26.4±5.2
carbon loss [Tg C/yr]							
SHAF		577±14.0	457±81.8	402±21.5	504±38.1	537±37.6	414±39.8
NHAF		621±69.0	280±36.7	308±21.2	490±79.5	510±88.9	367±71.3

* Lehsten et al. (2009) uses burned areas as reported in L3JRC modified by a correction term to compensate for a likely underestimation.

Table 3. Annual mean carbon in the above ground vegetation pools (deadstem, livestem, leaves, coarse woody debris and litter), annual burned area, and ratio between annual carbon loss and burned area in steady state for the different simulations.

	above veg.	annual burned area	annual carbon emission/ burned area
simulation	[Pg C]	[Mha]	[Tg C/Mha]
T-FULL	722	136	16.3
AB-FULL	579	300	8.5
AB-HI	649	194	9.4
AB-HI-FS	659	182	9.8

Table 4. Correlation coefficient for the interannual variability (1997–2004) between model simulations and GFEDv2 (van der Werf et al., 2006) and GICC (Mieville et al., 2010) for total (wildfire and deforestation) fire carbon emissions, relative standard deviation (relative sdev) of monthly fire carbon emissions for GFEDv2 or GICC, and the interannual correlation (correlation) between GFEDv2 and GICC. Non significant correlations (confidence level below 90%) are printed in cursive characters. Regions are defined in Fig. A3.

	Correlation – interannual variability								relative sdev		correlation
	T-FULL		AB-FULL		AB-HI		AB-HI-FS		Observations		
region	GFEDv2	GICC	GFEDv2	GICC	GFEDv2	GICC	GFEDv2	GICC	GFEDv2	GICC	GFEDv2/GICC
BONA	*0.47*	*0.26*	*0.37*	*0.21*	*0.32*	*0.16*	*0.30*	*0.12*	0.75	0.78	0.93
TENA	0.94	*0.38*	0.94	0.66	0.94	0.64	0.86	0.69	0.37	0.45	0.56
CEAM	0.83	0.87	0.81	0.83	0.79	0.82	0.80	0.82	1.17	0.76	0.95
NHSA	0.64	0.68	0.89	0.73	0.85	0.80	0.83	0.77	0.64	0.32	0.80
SHSA	*0.30*	0.61	*0.18*	0.61	*0.21*	0.63	*0.20*	0.62	0.31	0.27	0.70
EURO	*0.48*	*0.42*	0.74	0.68	0.73	0.65	0.80	0.68	0.37	0.35	0.86
MIDE	*−0.03*	*−0.25*	*0.36*	*0.24*	*0.38*	*0.28*	*0.42*	*0.15*	0.57	0.39	0.80
NHAF	*0.46*	*0.25*	*0.39*	*0.18*	*−0.32*	*0.29*	*0.24*	*0.17*	0.12	0.28	*−0.02*
SHAF	*0.36*	0.56	*0.01*	*0.30*	*−0.12*	*0.22*	*−0.01*	*0.23*	0.12	0.15	0.83
BOAS	*0.40*	*0.36*	*0.29*	*0.36*	*0.31*	*0.38*	*0.40*	*0.45*	0.70	0.70	0.81
CEAS	*−0.12*	*0.01*	*−0.19*	*0.21*	*−0.27*	*0.10*	*−0.21*	*0.09*	0.17	0.30	0.66
SEAS	*−0.03*	*−0.22*	0.58	*0.37*	0.56	*0.37*	0.54	*0.32*	0.63	0.36	0.94
EQAS	0.95	0.99	1.00	0.99	1.00	1.00	1.00	1.00	1.34	1.14	0.98
AUST	*0.21*	*0.15*	*0.09*	*−0.03*	*−0.11*	*−0.17*	*−0.12*	*−0.17*	0.24	0.27	0.80
GLOB	0.88	*0.29*	0.92	*0.37*	0.91	*0.37*	0.91	*0.35*	0.14	0.10	0.64

Table A1. Mortality (MORT) factors for different plant functional types and fuel types after Thonicke et al. (2001) and combustion completeness (CC) factors used in CLM-CN in combination with the Thonicke et al. (2001) algorithm.

PFT	CC Leaf	CC Stem	CC Root	CC Litter	CC CWD	MORT Leaf	MORT Stem	MORT Root
needleleaf evergreen temperate tree	1.0	0.2	0.2	1.0	0.2	0.78	0.78	0.78
needleleaf evergreen boreal tree	1.0	0.2	0.2	1.0	0.2	0.78	0.78	0.78
needleleaf deciduous boreal tree	1.0	0.2	0.2	1.0	0.2	0.78	0.78	0.78
broadleaf evergreen tropical tree	1.0	0.2	0.2	1.0	0.2	0.78	0.78	0.78
broadleaf evergreen temperate tree	1.0	0.2	0.2	1.0	0.2	0.50	0.50	0.50
broadleaf deciduous tropical tree	1.0	0.2	0.2	1.0	0.2	0.50	0.50	0.50
broadleaf deciduous temperate tree	1.0	0.2	0.2	1.0	0.2	0.78	0.78	0.78
broadleaf deciduous boreal tree	1.0	0.2	0.2	1.0	0.2	0.78	0.78	0.78
broadleaf evergreen shrub	1.0	0.2	0.2	1.0	0.2	0.78	0.78	0.78
broadleaf deciduous temperate shrub	1.0	0.2	0.2	1.0	0.2	0.78	0.78	0.78
broadleaf deciduous boreal shrub	1.0	0.2	0.2	1.0	0.2	0.78	0.78	0.78
c3 arctic grass	1.0	0.2	0.2	1.0	0.2	1.0	1.0	1.0
c3 non-arctic grass	1.0	0.2	0.2	1.0	0.2	1.0	1.0	1.0
c4 grass	1.0	0.2	0.2	1.0	0.2	1.0	1.0	1.0

Table A2. Combustion Completeness (CC) and Mortality (MORT) factors for different plant functional types and fuel types after Arora and Boer (2005).

PFT	CC Leaf	CC Stem	CC Root	CC Litter	CC CWD	MORT Leaf	MORT Stem	MORT Root
needleleaf evergreen temperate tree	0.8	0.5	0.0	0.5	0.5	0.9	0.8	0.1
needleleaf evergreen boreal tree	0.8	0.5	0.0	0.5	0.5	0.9	0.8	0.1
needleleaf deciduous boreal tree	0.8	0.5	0.0	0.5	0.5	0.9	0.8	0.1
broadleaf evergreen tropical tree	0.8	0.5	0.0	0.6	0.6	0.9	0.8	0.1
broadleaf evergreen temperate tree	0.8	0.5	0.0	0.6	0.6	0.9	0.8	0.1
broadleaf deciduous tropical tree	0.8	0.5	0.0	0.6	0.6	0.9	0.6	0.1
broadleaf deciduous temperate tree	0.8	0.5	0.0	0.6	0.6	0.9	0.6	0.1
broadleaf deciduous boreal tree	0.8	0.5	0.0	0.6	0.6	0.9	0.6	0.1
broadleaf evergreen shrub	0.8	0.5	0.0	0.6	0.6	0.9	0.6	0.1
broadleaf deciduous temperate shrub	0.8	0.5	0.0	0.6	0.6	0.9	0.8	0.1
broadleaf deciduous boreal shrub	0.8	0.5	0.0	0.6	0.6	0.9	0.8	0.1
c3 arctic grass	0.9	0.0	0.0	0.7	0.7	0.9	0.0	0.25
c3 non-arctic grass	0.9	0.0	0.0	0.7	0.7	0.9	0.0	0.25
c4 grass	0.9	0.0	0.0	0.7	0.7	0.9	0.0	0.25

Table A3. The redistribution of carbon and nitrogen upon conversion used in CLM-CN. Factors are based on Houghton et al. (1983).

Ecosystem	conversion flux	paper product pool	wood product pool
Temperate/boreal forest	0.60	0.30	0.10
Tropical forest	0.60	0.40	0.00
Grassland	1.00	0.00	0.00
Shrub lands	0.80	0.20	0.00

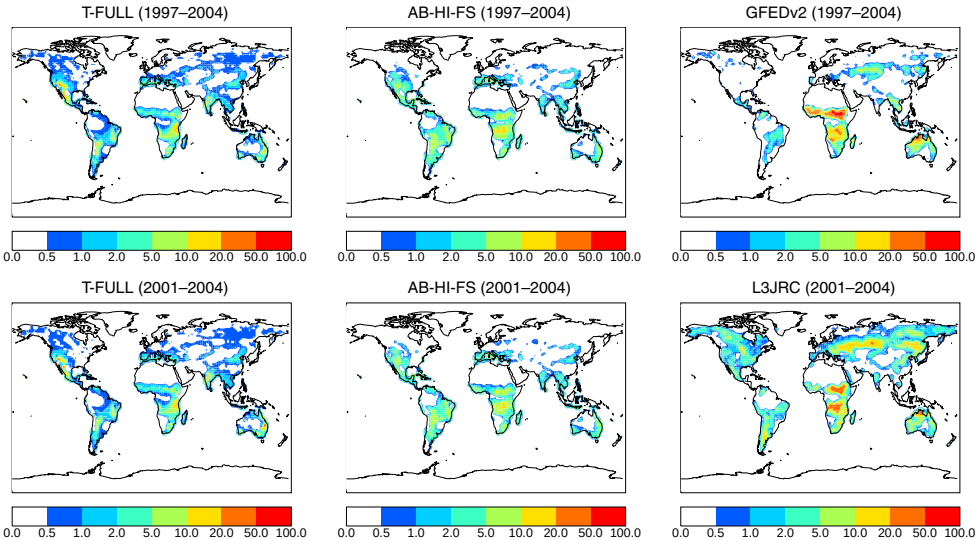

Fig. 1. Simulated annual total (wildfire plus deforestation) area burned [percentage of grid box] compared to satellite based fire products: GFEDv2 (van der Werf et al., 2006) and L3JRC (Tansey et al., 2008). The model simulations are averaged over the corresponding observational periods (GFEDv2: 1997–2004; L3JRC: 2001–2004). Regional values for all simulations performed are given in Fig. 2.

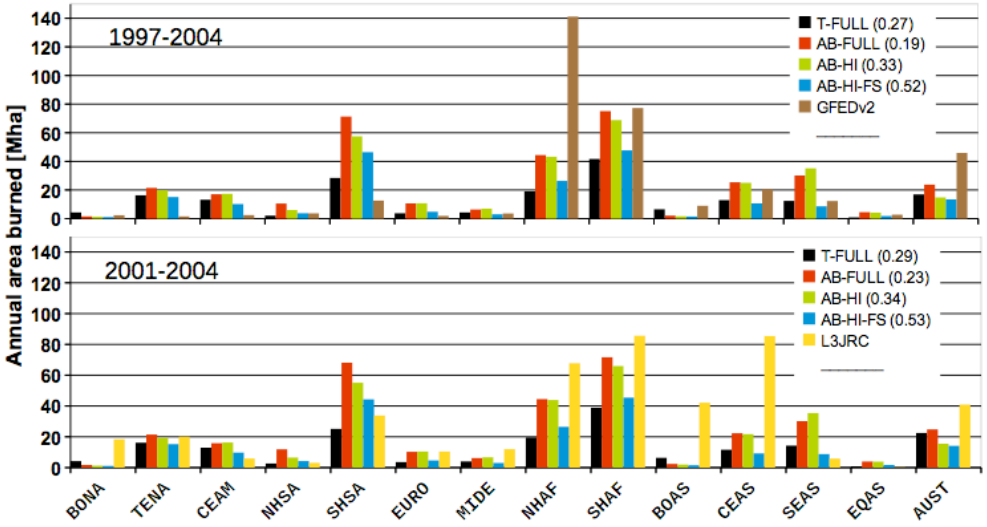

Fig. 2. Annual mean total area burned (wildfire plus deforestation) in [Mha] for different regions compared to GFEDv2 (van der Werf et al., 2006) and L3JRC (Tansey et al., 2008). The model simulations are averaged over the corresponding observational period (1997–2004, 2001–2004, respectively). The number in brackets denote spatial correlation coefficients between simulations and satellite based fire products. Regions are defined in Fig. A3.

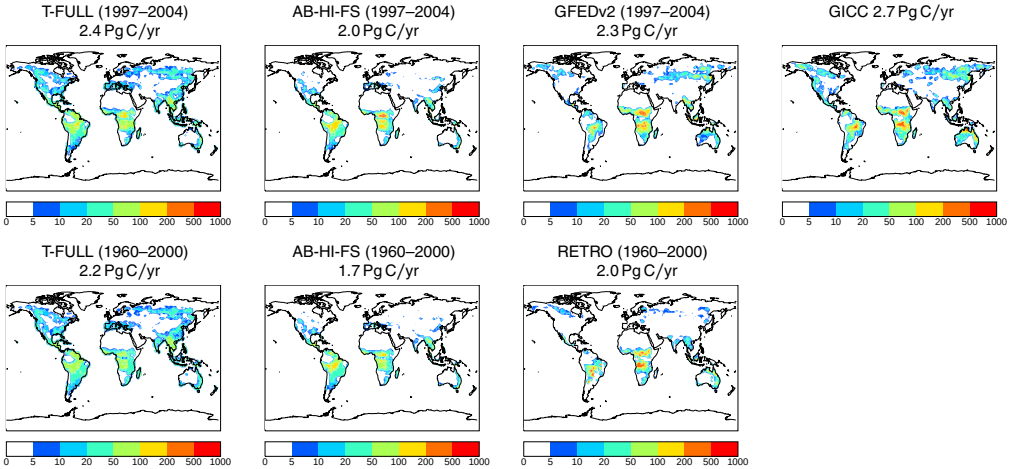

Fig. 3. Annual mean total (wildfire plus deforestation) fire carbon emissions [g C/m^2/year] compared to emissions reported in the fire products GFEDv2 (van der Werf et al., 2006), RETRO (Schultz et al., 2008) and GICC (Mieville et al., 2010). The model simulations are averaged over the corresponding observational periods (GFEDv2/GICC: 1997–2004; RETRO: 1960–2000). Numbers report global total carbon emissions. Regional values for all simulations performed are given in Fig. 4.

BGD
7, 565–630, 2010

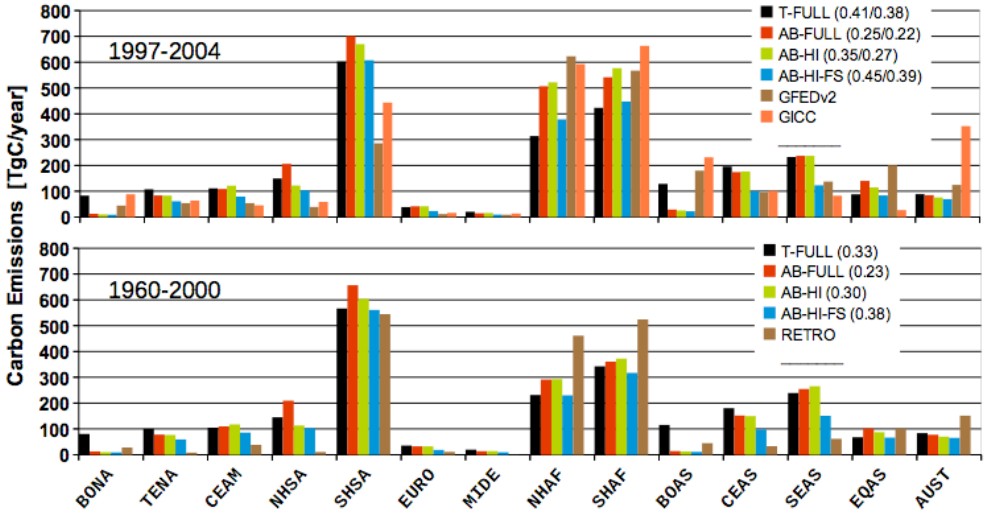

Fig. 4. Annual mean total (wildfire plus deforestation) fire carbon emissions in [Tg C/year] for different regions compared to GFEDv2 (van der Werf et al., 2006), GICC (Mieville et al., 2010), and RETRO (Schultz et al., 2008). The model simulations are averaged over the corresponding observational period (1997–2004 or 1960–2000, respectively). The number in brackets denote global spatial correlation coefficients between simulations and fire products (for the upper panel the first numbers refers to GFEDv2 and the second to GICC). Regions are defined in Fig. A3.

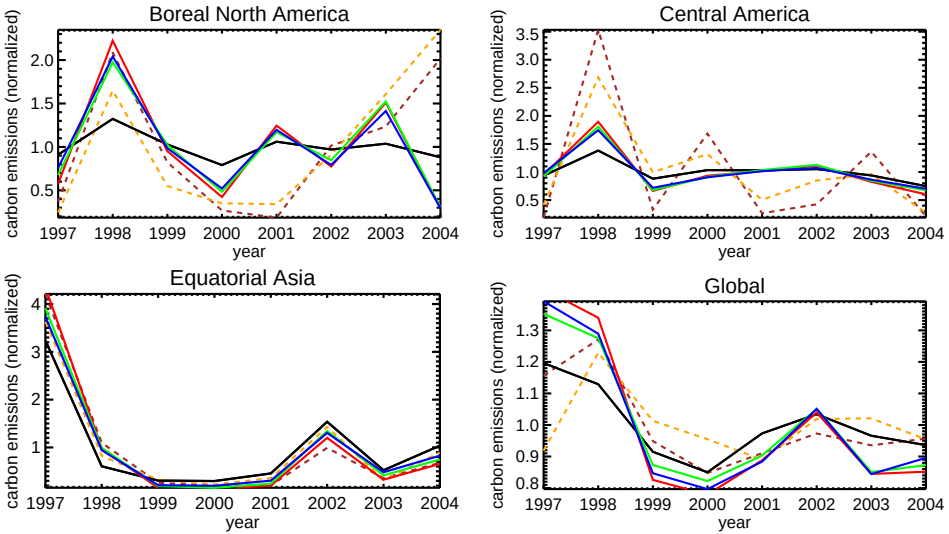

Fig. 5. Annual mean total (wildfire and deforestation) fire carbon emissions normalized by the mean for 1997–2004 for regions characterized by a high interannual variability reported in the satellite based products and globally. Solid lines represent model simulations: black: T-FULL, red: AB-FULL, green: AB-HI; blue: AB-HI-FS. Dashed lines are observations: brown: GFEDv2 (van der Werf et al., 2006); orange: GICC (Mieville et al., 2010). Correlation coefficients for the interannual variability for different regions are given in Table 4.

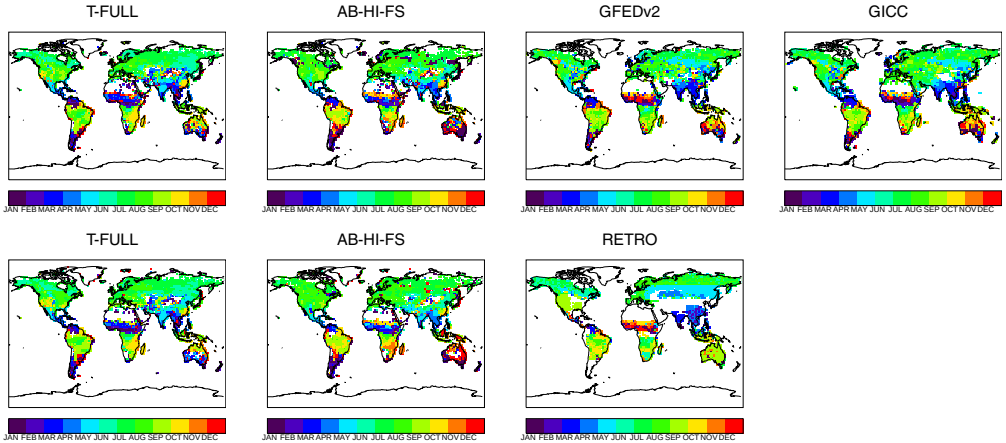

Fig. 6. Month of maximum total (wildfire plus deforestation) fire carbon emissions for the different simulations compared to different fire products: GFEDv2 (van der Werf et al., 2006), GICC (Mieville et al., 2010) and RETRO (Schultz et al., 2008). The model simulations are averaged over the corresponding observational periods (GFEDv2, GICC: 1997–2004; RETRO: 1960–2000).

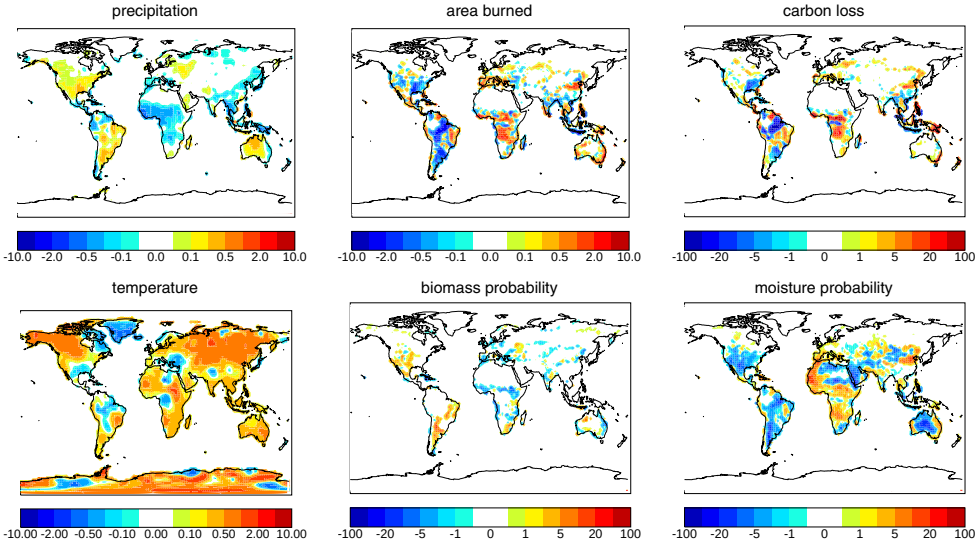

Fig. 7. Difference between simulation AB-FULL and AB-CLIM in annual mean temperature [K], annual mean precipitation [mm/d], annual total area burned [% of grid box], annual mean carbon emissions [g C/m^2/year] and biomass and moisture probability [*100] as defined in A2 averaged over the period 1973–1997.

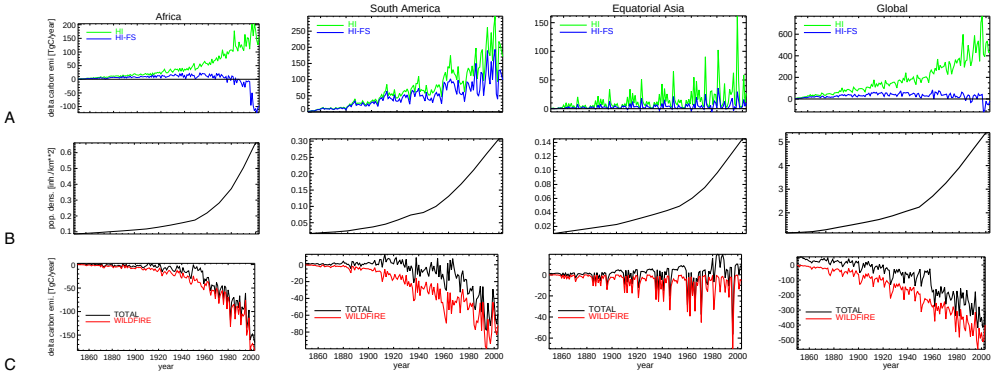

Fig. 8. Sensitivity to changes in population density and land use change and wood harvest for selected regions and globally. A: Annual mean change in carbon emission from total fires (natural and deforestation) caused by changes in population density in the case of only human ignition is considered (green line, AB-HI – AB-HI-PI) and human ignition and fire suppression considered (blue line, AB-HI-FS – AB-HI-FS-PI) in [Tg C/year]; B: population density [inhabitants/km^2]; C: change in total (wildfire and deforestation) fire carbon emissions (black) and wildfire fire carbon emissions (red) caused by land use change and wood harvest in [Tg C/year] (AB-FULL – AB-LUC).

BGD
7, 565–630, 2010

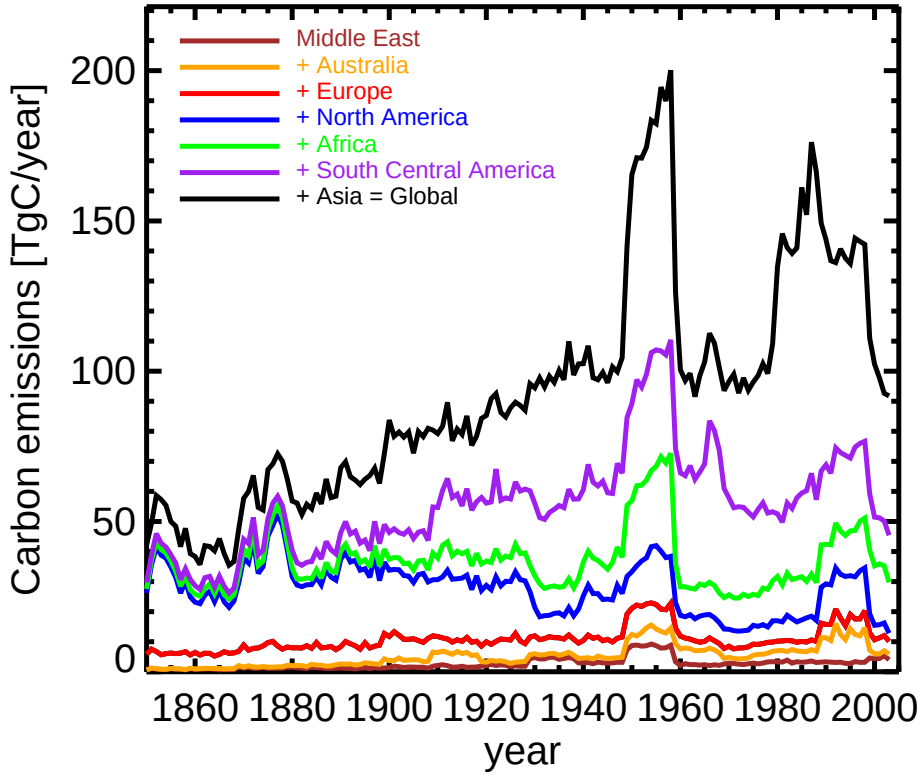

Fig. 9. Annual mean fire emissions from deforestation [Tg C/year] as simulated in simulation AB-FULL. The contribution of each region is stacked onto the region plotted below, so that the black line represents the global deforestation carbon loss.

BGD
7, 565–630, 2010

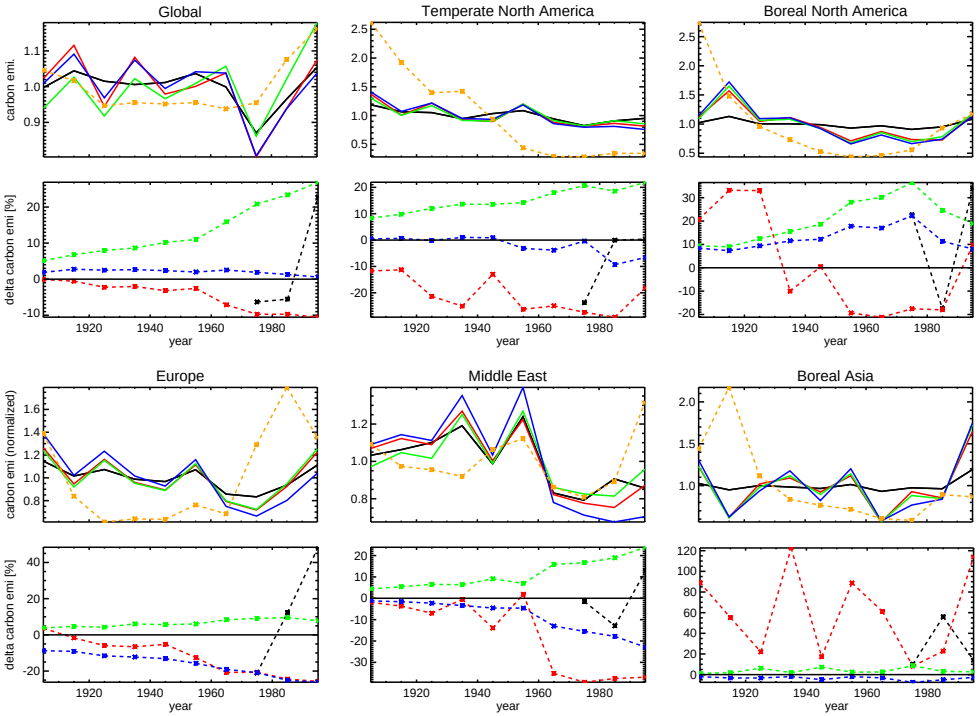

Fig. 10. Upper panels: Trend in decadal total (wildfire and deforestation) fire carbon emissions compared to decadal mean GICChist estimates (Mieville et al., 2010) for different regions from 1900 to 2000 normalized with the mean value for 1900–2000. Solid lines represent model simulations: black: T-FULL, red: AB-FULL, green: AB-HI; blue: AB-HI-FS. Dashed orange line with symbols are observations (GICChist); Lower panels: decadal mean change in total carbon loss in [%] with respect to the respective control simulation caused by red: land use change and wood harvest, green: human ignition, blue: human ignition and fire suppression, black: climate. Note here, that the fire carbon-system is highly non-linear and therefore the individual responses are not additive.

BGD
7, 565–630, 2010

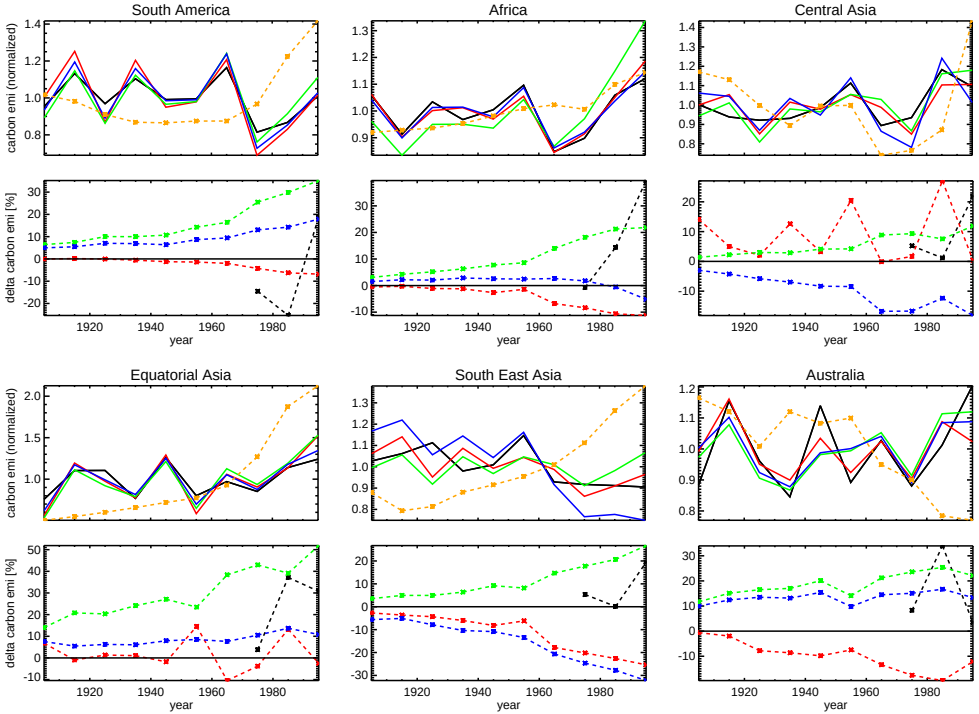

Fig. 10. Continued.

BGD
7, 565–630, 2010

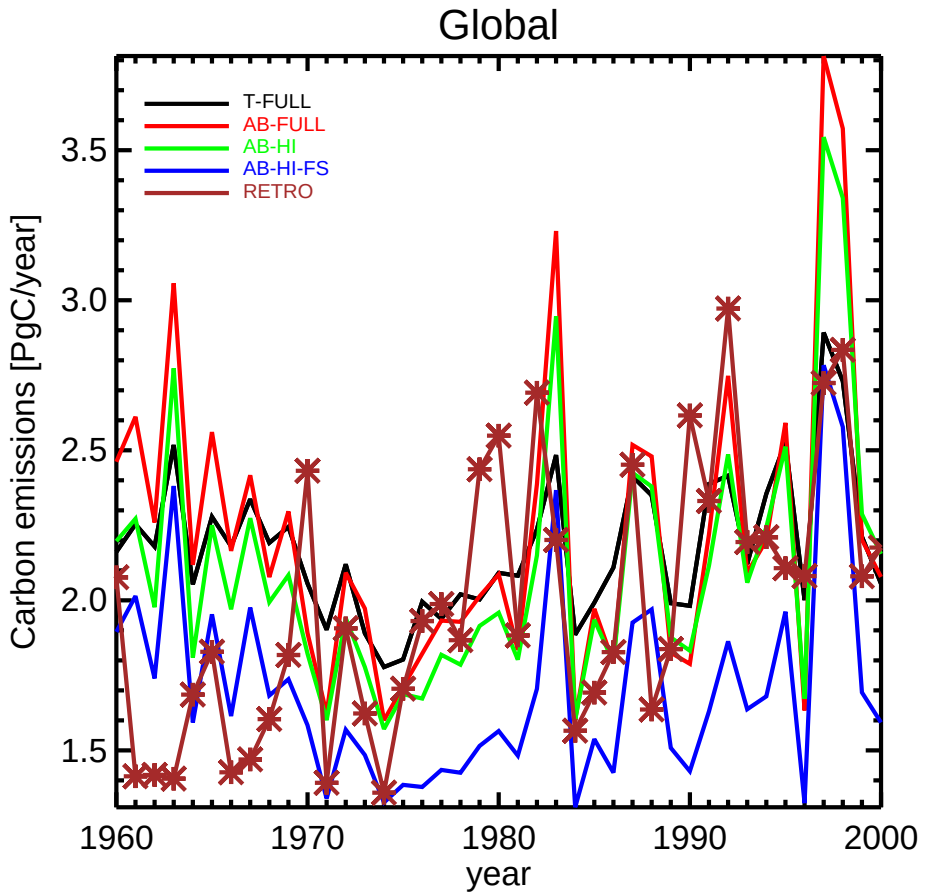

Fig. 11. Annual mean total (wildfire and deforestation) fire carbon emissions in [Pg C/year] for the different simulations from 1960–2000 compared to values reported in RETRO (Schultz et al., 2008).

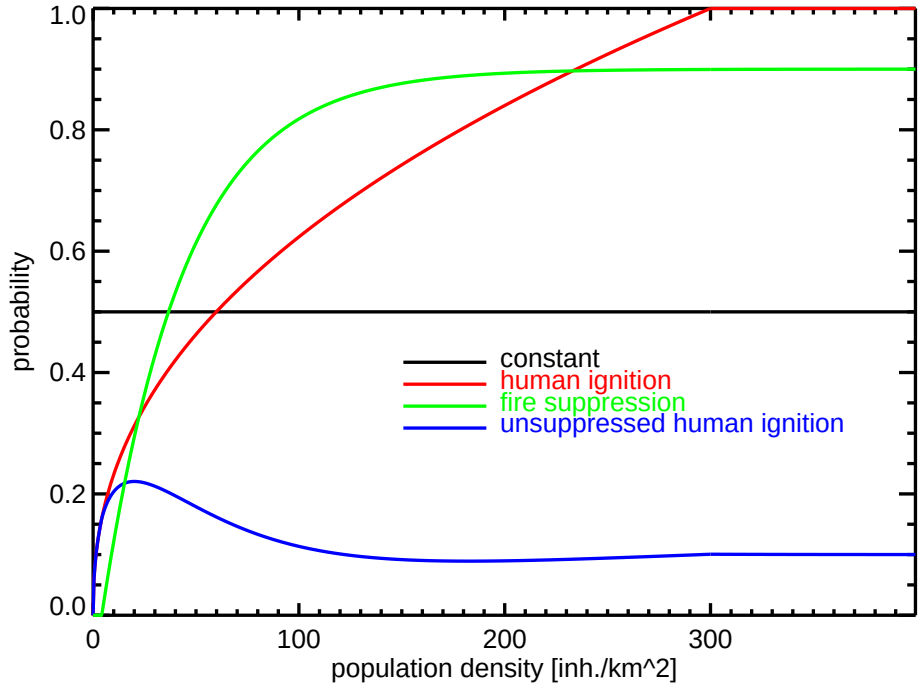

Fig. A1. Human ignition probability and fire suppression [0–1] as function of population density [inhabitants/km^2]. Black: constant ignition probability; red: Human ignition probability; green: fire suppression; blue: unsuppressed human ignition (human ignition$*$(1−fire suppression)).

BGD
7, 565–630, 2010

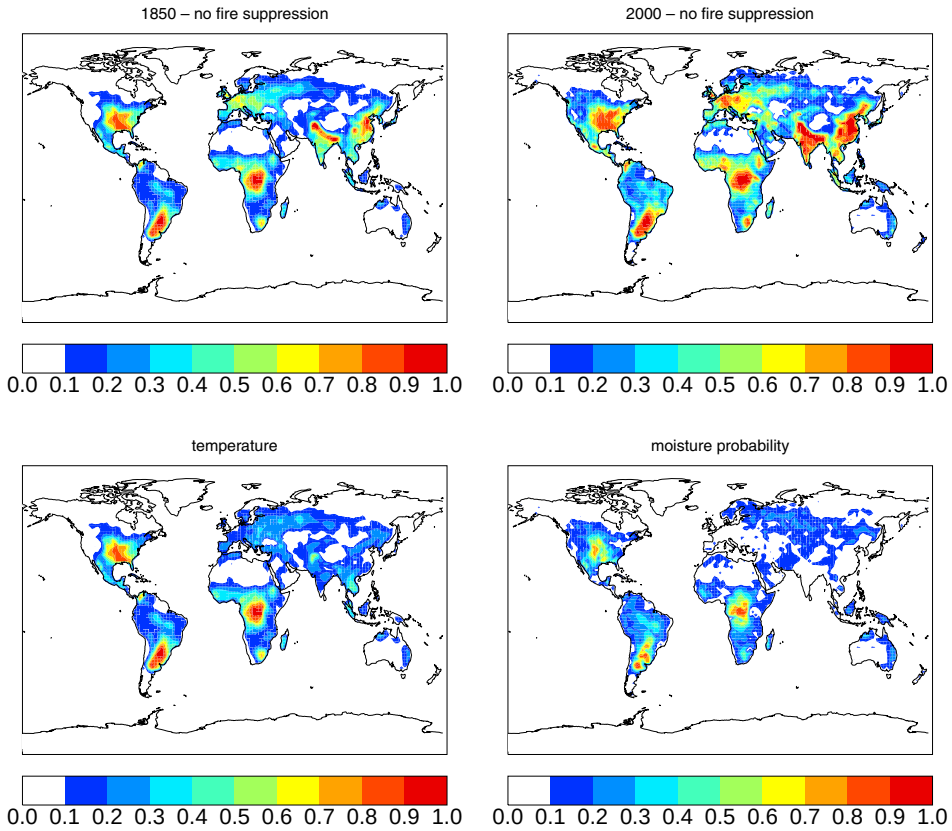

Fig. A2. Annual mean total ignition probability for the years 1850 and 2000 with and without fire suppression considered.

BGD
7, 565–630, 2010

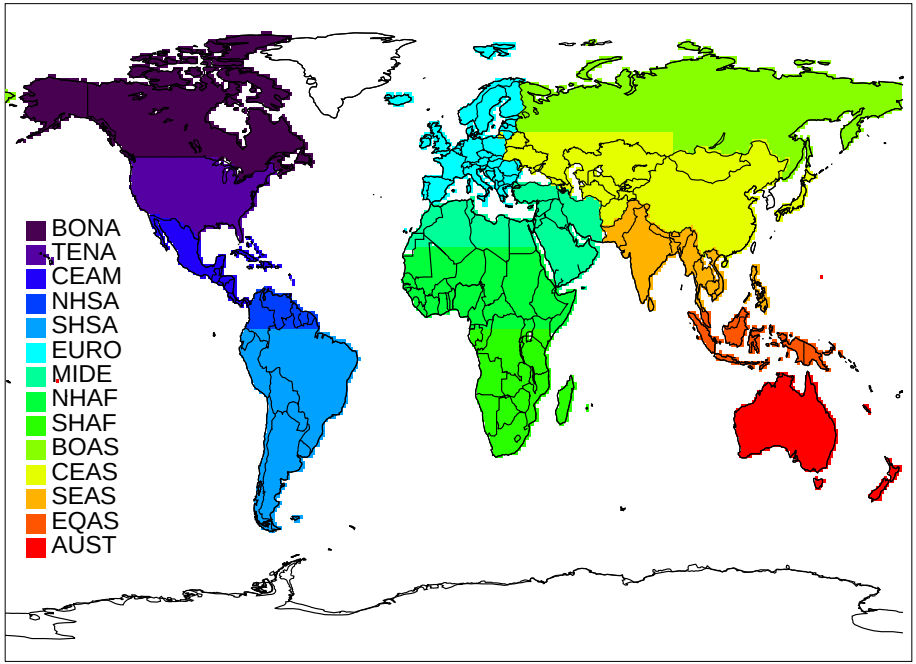

Fig. A3. Map of the 14 regions as defined in van der Werf et al. (2006) used in this study. BONA: Boreal North America, TENA: Temperate North America, CEAM: Central America, NHSA: Northern Hem. South America, SHSA: Southern Hem. South America, EURO: Europe, MIDE: Middle East, NHAF: Northern Hem. Africa, SHAF: Southern Hem. Africa, BOAS: Boreal Asia, CEAS: Central Asia, SEAS: South East Asia, EQAS: Equatorial Asia, AUST: Australia.